A tomato B-box protein regulates plant development and fruit quality through the interaction with PIF4, HY5 and RIN transcription factors

Lumi Shiose[1,§], Juliene dos Reis Moreira[1,§], Bruno Silvestre Lira[1], Gabriel Ponciano[1], Gabriel Gomez Ocampo[2], Raquel Tsu Ay Wu[1], José Laurindo dos Santos Júnior[1], Nikolaos Ntelkis[3], Elke Clicque[3], Maria José Oliveira[1], Greice Lubini[4], Eny Iochevet Segal Floh[1], Javier Francisco Botto[2], Marcelo José Pena Ferreira[1], Alain Goossens[3], Luciano Freschi[1], Magdalena Rossi[1,‡]

Author affiliations:

[1] Departamento de Botânica, Instituto de Biociências, Universidade de São Paulo, Rua do Matão 277, 05508-090, São Paulo, Brasil.

[2] IFEVA, Facultad de Agronomía, Universidad de Buenos Aires y Consejo Nacional de Investigaciones Científicas y Técnicas, Avenida San Martín 4453, Buenos Aires C1417DSE, Argentina.

[3] Department of Plant Systems Biology, VIB, UGent-Plant Biotechnology and Bioinformatics, Technologiepark 927, B-9052 Gent, Belgium,

[4] Departamento de Biologia, Faculdade de Filosofia, Ciências e Letras de Ribeirão Preto, Universidade de São Paulo, Avenida Bandeirantes 3900, 14040-901, Ribeirão Preto, Brasil.

[§] Both authors contributed equally.

[‡] Corresponding author

Highlight

Through the interaction with master transcription factors of light signaling and ripening, tomato SlBBX20 protein regulates vegetative and reproductive growth contributing to determine yield and fruit quality.

Abstract

During the last decade, the knowledge about BBX proteins has abruptly increased. Genome-wide studies identified BBX gene family in several ornamental, industry and food crops; however, the reports regarding the role of these genes as regulators of agronomically important traits are scarce. Here, by phenotyping a knockout mutant, we performed a comprehensive functional characterization of the tomato locus Solyc12g089240, hereafter called *SlBBX20*. The data revealed the encoded protein as a positive regulator of light signaling affecting several physiological processes during plant lifespan. By the inhibition of PHYTOCHROME INTERACTING FACTOR 4 (SlPIF4)-auxin crosstalk, SlBBX20 regulates photomorphogenesis. Later, it controls the balance between cell division and expansion to guarantee the correct vegetative and reproductive development. In fruits, SlBBX20 is transcriptionally induced by the master transcription factor RIPENING INHIBITOR (SlRIN) and, together with ELONGATED HYPOCOTYL 5 (SlHY5), upregulates flavonoids biosynthetic genes. Finally, SlBBX20 promotes the accumulation of steroidal glycoalkaloids and attenuates *Botrytis cinerea* infection. This work clearly demonstrates that BBX proteins are multilayer regulators of plant physiology, not only because they affect multiple processes along plant development but also regulate other genes at the transcriptional and post-translational levels.

Keywords: BBX proteins, hypocotyl elongation, light signaling, photomorphogenesis, plant defense, ripening, shade avoidance, *Solanum lycopersicum*, specialized metabolism, tomato.

INTRODUCTION

Initially characterized in *Arabidopsis thaliana* as pivotal factors in light-signaling, plant BBX proteins have drawn attention during the last few years due to their involvement in several developmental processes, including seed germination, seedling photomorphogenesis, thermomorphogenesis, floral transition, shade avoidance, senescence and, even, responses to biotic and abiotic stresses (Talar and Kiełbowicz-Matuk, 2021; Cao *et al.*, 2023). BBX proteins are zinc finger transcription factors (TFs) characterized by the presence of one or two B-box domains, which play a paramount role in protein-protein interaction. Additionally, some BBXs contain the CONSTANS, CONSTANS-like and TIMING OF CAB1 (CCT) domain in the carboxyl terminus of the protein (Gangappa and Botto, 2014). The members of this protein family regulate transcription either by direct interaction with target gene promoters (Tiwari *et al.*, 2010; Xu *et al.*, 2016) or by modifying the transcriptional regulatory activity of other TFs through heterodimerization (Tripathi *et al.*, 2017; Song *et al.*, 2020).

Recently, genome-wide surveys have identified BBX protein encoding genes in several economically important plant species, such as wild peanut *Arachis duranensis* (Jin *et al.*, 2019), sweet cherry (Y. Wang *et al.*, 2021a), *Gossypium* sp. (Feng *et al.*, 2021), *Iris germanica* (Y. Wang *et al.*, 2021b), cucumber (Obel *et al.*, 2022), rice/maize/sorghum/stiff brome/millet (Huang *et al.*, 2012; Shalmani *et al.*, 2019), potato (Talar *et al.*, 2017), apple (Liu *et al.*, 2018), orchid *Dendrobium officinale* (Cao *et al.*, 2019), grapevine (Wei *et al.*, 2020), pepper (Wang *et al.*, 2022), pear (Cao *et al.*, 2017), quinoa (Xuefen *et al.*, 2022), soybean (Shan *et al.*, 2022), *Saccharum spontaneum* (Wu *et al.*, 2023), sweet potato ancestor *Ipomoea trifida* (Hou *et al.*, 2021), *Nicotiana tabacum* (Song *et al.*, 2022), strawberry (Xu *et al.*, 2023a), yam (Chang *et al.*, 2023) and tomato (Lira *et al.*, 2020). However, the functional characterization of BBX proteins related to crop yield and quality traits remains scarce.

Particularly in tomato, out of the 31 BBX protein-encoding genes identified (Lira *et al.*, 2020), six were characterized as regulators of agronomically important traits. Beyond photomorphogenesis, SlBBX4 (Solyc08g006530) participates in the determination of flowering time, as evidenced by the higher number of leaves until the first anthesis observed in *Slbbx4* mutant genotype (Xu *et al.*, 2023b). Cui *et al.* (2022) demonstrated that SlBBX3/SlCOL1 (Solyc02g089540) affects yield by directly downregulating the expression of *SINGLE FLOWER TRUSS* (*SlSFT*) florigen, consequently delaying flowering and reducing flower number. In contrast, *SlBBX28* (Solyc12g005660) was found to be a positive regulator of flower and fruit number, acting downstream of *SlSFT*. By the upregulation of auxin metabolism and transcriptional repression of *FRUITFULL2* (*SlFUL2*), SlBBX28 determines the proper inflorescence branching pattern. Moreover, the SlBBX28-mediated auxin synthesis and signaling regulate vegetative growth (Lira *et al.*, 2022). Not only yield-related characters are regulated by

SlBBXs, but also fruit quality traits, as the content of nutraceutical compounds. In this sense, plants overexpressing *SlBBX25* (Solyc01g110180, although it was named *SlBBX20* by the authors, the locus corresponds to *SlBBX25* according to the first report of tomato BBX proteins, Chu *et al.*, 2016) developed dark green fruits and leaves, and ripe fruits with higher levels of carotenoids and flavonoids relative to the wild type counterparts. Further experiments demonstrated that SlBBX25 modulates pigment accumulation in a light-mediated manner (Xiong *et al.*, 2019; Luo *et al.*, 2021). Finally, SlBBXs have also been shown to participate in the response to environmental biotic and abiotic cues. *SlBBX25* negatively regulates resistance to *Botrytis cinerea* (Luo *et al.*, 2023). *SlBBX17* (Solyc07g052620) is upregulated by high temperature, and its overexpression confers heat tolerance with a dramatic gibberellin-mediated growth penalty (Xu *et al.*, 2022). *SlBBX17* expression is also induced by low temperatures conferring resistance in an ELONGATED HYPOCOTYL 5 (SlHY5)-dependent manner (Song *et al.*, 2023). Similarly, the overexpression of *SlBBX31* (Solyc07g053140) confers cold tolerance. Through a genome-wide association study in wild and cultivated tomato accessions, Zhu *et al.* (2023) discovered an insertion of 27 bp in the promoter of *SlBBX31* that impairs SlHY5-mediated transcriptional induction in response to chilling temperatures has been negatively selected during domestication. In a previous work, we have characterized the expression profile of several *SlBBXs* (Lira *et al.*, 2020). The mRNA levels of *SlBBX19* (Solyc01g110370), *SlBBX20* (Solyc12g089240), *SlBBX22* (Solyc07g062160), *SlBBX24* (Solyc06g073180) and *SlBBX26* (Solyc10g006750) increase from immature green towards red ripe stages of fruit development (Supplementary Fig. S1). *SlBBX20* shows the highest absolute expression and induction; moreover, its promoter binds RIPENING INHIBITOR (SlRIN), the master TF of tomato fruit ripening (Vrebalov *et al.*, 2002). Here, by the comprehensive phenotypic characterization of a knockout mutant, we demonstrate that SlBBX20 participates in light signaling, regulating several development processes, from seedling establishment to fruit ripening, positively impacting crop yield and fruit quality.

MATERIALS AND METHODS

Plant material and growth conditions

Solanum lycopersicum (cv. Micro-Tom) wild type (WT) harboring the wild allele of *GOLDEN2-LIKE 2* (*SlGLK2*) gene (Nguyen *et al.*, 2014) and *Slrin* mutant genotypes were obtained from the Laboratory of hormonal control of plant development, University of São Paulo (https://www.esalq.usp.br/tomato/).

Nicotiana benthamiana and tomato plants were grown in 6 L pots containing a 1:1 mixture of commercial substrate (Plantmax HT, Eucatex, Brazil) and vermiculite supplemented with 1 g L^{-1} of NPK 10:10:10, 4 g L^{-1} of dolomite limestone and 2 g L^{-1} of Yoorin Master® (Yoorin Fertilizantes, Brazil). Cultivation was carried out in a biosafety risk I greenhouse with manual

irrigation by capillarity under controlled temperature (25 ± 3 °C day and 20 ± 3 °C night) and natural light conditions (11.5 h/13 h photoperiod in winter/summer, respectively, and 250-350 μmol m^{-2} s^{-1} of incident photo irradiance).

Subcellular localization and bimolecular fluorescence complementation (BiFC)

Subcellular localization was predicted using cNLS Mapper (http://nls-mapper.iab.keio.ac.jp, Kosugi *et al.*, 2009), BaCelLo (http://gpcr.biocomp.unibo.it/bacello/, Pierleoni *et al.*, 2006) and DeepLoc 2.0 (https://services.healthtech.dtu.dk/services/DeepLoc-2.0/; Thumuluri *et al.*, 2022). The full-length open reading frame of *SlBBX20* (Solyc12g089240), *SlBBX26* (Solyc10g006750, as interaction negative control), *SlPIF4* (Solyc07g043580) and *SlRIN* (Solyc05g012020) without stop codon were amplified using specific primers listed in Supplementary Table S1 and cloned into pCR™ 8/GW/TOPO TA Cloning (Invitrogen) entry vector. For subcellular localization, *SlBBX20* coding region was recombined into the binary vector pK7FWG2 (Karimi *et al.*, 2002) using LR clonase II enzyme mix (Invitrogen). Since SlBBX20 showed autoactivation when fused to the GAL4 DNA-binding domain of the Y2H system, its homodimerization was assessed by bimolecular fluorescence complementation assay (BiFC). *SlBBX20, SlBBX26, SlPIF4* and *SlRIN* coding regions were recombined into pDEST-GWVYNE or pDEST-GWVYCE vectors (Gehl *et al.*, 2009) using LR clonase II enzyme mix (Invitrogen). The binary vectors were introduced in *Agrobacterium tumefaciens* strain GV3101. Cultures were resuspended in infiltration buffer (50 mM MES pH 5.6, 2 mM sodium phosphate buffer pH 7, 0.5% glucose and 200 μM acetosyringone (Sigma-Aldrich)) to a final OD600 of 0.5, incubated for 3 h in the dark at room temperature and infiltrated into leaves of 4-week-old *Nicotiana benthamiana* plants. DAPI (4′,6-diamidino-2-phenylindole) was used as a nuclear marker. Confocal analyses for subcellular localization and BiFC were carried out as described in Lira *et al.* (2017) in a Leica TCS SP8 STED 3X confocal system coupled to a Leica DMi 8 microscope (CAIMi IB-USP). GFP and YFP signals were captured over a 508- to 553-nm range after excitation at 488 nm.

Generation of *SlBBX20* CRISPR/Cas9 knockout line

Slbbx20 mutant tomato plants were obtained by CRISPR/Cas9 system in *Solanum lycopersicum* (cv. Micro-Tom) background. Two gRNAs sequences were inserted into pDIRECT_22C vector expressing the Csy4-multi-gRNA system (Čermák *et al.*, 2017) to simultaneously target two sites in *SlBBX20* (Supplementary Table S1). Tomato plants were stably transformed with the construct via *Agrobacterium tumefaciens*-mediated transformation according to Pino *et al.* (2010). The presence of the vector T-DNA was confirmed by PCR using primers: (i) TC320 and M13F anchored to the CmYLCV promoter and CSY terminator, respectively and; (ii) Cas9 coding region (Supplementary Table S1). Cas9-mediated editions were analyzed in T0 regenerated plants by PCR with BBX20 specific primers followed by Sanger sequencing (Supplementary Table S1).

The T-DNA was segregated in T2 generation, and all experiments were performed with T4 homozygous mutants.

Hypocotyl elongation assay

WT and mutant *Slbbx*20 seeds were surface sterilized with 30% (v/v) commercial bleach (2.7% w/v sodium hypochlorite) for 15 min in agitation, rinsed with distilled water and inoculated in square culture vessels (16 vessels with 16 seeds each per genotype) containing sterile medium composed of 1/2X MS (Murashige and Skoog, 1962) and 2% (w/v) phytagel. The pH was adjusted to 5.7 ± 0.05. The seeds were kept in darkness for four days at 25 ± 2 °C to synchronize germination. After germination, at the fifth day, eight vessels per genotype were transferred to continuous white light (100 μmol m^{-2} s^{-1}, R/FR: 2.3), and eight were maintained under absolute darkness for another four days. At the eighth day, the length of the hypocotyls after light or dark treatment, was measured, and five biological replicates of pooled hypocotyls/cotyledons were sampled for each treatment/genotype, frozen in liquid nitrogen and stored at -80 °C for further analysis.

Reverse transcriptase and quantitative PCR (RT-qPCR) analysis

RNA extraction, complementary DNA (cDNA) synthesis, and qPCR assays were performed as described by Quadrana *et al.*, (2013). Primer sequences and loci IDs are detailed in Supplementary Table S1. qPCR reactions were carried out in a QuantStudio 6 Flex Real-Time PCR system (Applied Biosystems) using 2X Power SYBR Green Master Mix reagent (Life Technologies) in a 10 μL final volume. Absolute fluorescence data were analyzed using the LinRegPCR software package (Ruijter *et al.*, 2009) to obtain cycle quantitation (Cq) values and calculate PCR efficiency. Expression values were normalized against the geometric mean of two reference genes, *SlTIP41* and *SlEXPRESSED*, according to Quadrana *et al.* (2013). A permutation test lacking sample distribution assumption (Pfaffl *et al.*, 2002) was applied to detect statistical differences ($P \leq 0.05$) in expression ratios using the algorithms in the fgStatistics software package (Di Rienzo, 2009).

Yeast two-hybrid (Y2H)

The complete coding sequence of *SlBBX20* (Solyc12g089240) was cloned into pGADT7 Gateway™ vector at the N-terminus of the activation domain (AD) of the GALACTOSIDASE 4 (GAL4) transcriptional activator. *SlHY5* (Solyc08g061130), *SlPIF4* (Solyc07g043580) and *SlRIN* (Solyc05g012020) interactors were cloned into pGBT9 Gateway™ vector at the N-terminus of GAL4 DNA-binding domain (BD) (Cuéllar *et al.*, 2013). *Saccharomyces cerevisiae* PJ69-4A strain (James *et al.*, 1996) was co-transformed with both destination vectors using polyethylene glycol (PEG)/lithium acetate method. Transformants were selected on SD (synthetic minimal)

medium (Takara Bio, Shigo, Japan) lacking Leucine and Tryptophan. Three individual colonies were grown overnight in liquid cultures at 30 °C and 10- or 100-fold dilutions were dropped on control (SD-Leu-Trp) and selective media (SD-Leu-Trp-His).

As SlBBX20 fused to BD showed self-activation all assays were conducted with this protein fused to AD. For SlBBX20 and SlRIN interaction 60 mM of the autoactivation inhibitor 3-aminotriazole was used.

Transient expression assay (TEA)

For transient expression assays, the coding sequence of *SlBBX20, SlPIF4, SlHY5* and *SlRIN* were PCR-amplified from leaf cDNA with the primers listed in Supplementary Table S1 and cloned into pCR™ 8/GW/TOPO TA Cloning vector (Invitrogen). Subsequently, a Gateway LR II recombination reaction (Invitrogen) was performed with the p2GW7 vector (Vanden-Bossche *et al.*, 2013), obtaining the effector constructs. The *SlBBX20* (977 bp), *SlPIF4* (1617 bp), *SlCHS1* (1170 bp), *SlCHI2* (1232 bp), *SlF3H* (926 bp) and *SlFLS* (1114 bp) promoter regions were PCR-amplified from leaf gDNA and cloned into pCR™ 8/GW/TOPO TA Cloning vector (Invitrogen). Next, Gateway LR II recombination reaction (Invitrogen) was performed with the pGWL7 vector (Vanden-Bossche *et al.*, 2013), obtaining the promoter constructs harboring *FIREFLY LUCIFERASE* (*fLUC*) reporter gene. Transient expression assays were performed in protoplasts prepared from *Nicotiana tabacum* Bright Yellow-2 (BY-2) cells, as previously described Vanden-Bossche *et al.* (2013). Briefly, protoplasts were transfected with promoter/effector combinations. For normalization, a construct with RENILLA (*rLUC*) reporter gene under the control of *CaMV35S* promoter was co-transfected. As negative control, instead of effector, a construct containing *pCaMV35S*::*GUS* was used. fLUC activity was expressed as fLUC/rLUC activity ratio relative to negative control.

Shade avoidance response assay

WT and mutant *Slbbx*20 seeds were sown in sowing trays with 1:1 mixture of commercial substrate (Plantmax HT, Eucatex, Brazil) and vermiculite, maintained for four days in darkness for germination, kept for two days in constant white light for deetiolation and then submitted to white light (control)/shade treatment for 15 days. The white light treatment (WL) consisted in a combination of full spectrum, warm and far-red LEDs with a neutral filter: photosynthetically active radiation (PAR) = 40 μmol m^{-2} s^{-1}, red = 7.6 μmol m^{-2} s^{-1}, blue = 1.9 μmol m^{-2} s^{-1}, far-red = 12.2 μmol m^{-2} s^{-1}. The shade light treatment was obtained with the same source of WL and a green acetate filter (#089; LEE Filters, http://www.leefilters.com): PAR= 40 μmol m^{-2} s^{-1}, red = 4.0 μmol m^{-2} s^{-1}, blue = 1.9 μmol m^{-2} s^{-1}, far-red = 22.0 μmol m^{-2} s^{-1}. The R/FR ratios were 0.6 and 0.1 in WL and shade, respectively. Both treatments were performed at 25 ± 0.5 °C. Hypocotyl length was measured until reaching the plateau (maximum length, 6 days after white/shade light

treatment). At the end of the treatment, the plant height and the first internode length were scored. Moreover, the mRNA level of the SAR inhibitor *PHYTOCHROME RAPIDLY REGULATED 1* (*SlPAR1*) was profiled in primordia (≤ 1 cm) , young (≤ 2 cm) and expanding (≤ 3 cm) leaves.

Experimental planting and sampling for phenotypic characterization

For *Slbbx20* mutant phenotypic characterization, several experiments were carried out.

For vegetative growth evaluation (Fig. 2A), 20 plants per genotype were grown for 55 days. Total leaf number, leaf area and dry weight were recorded. Total leaf area was obtained by digitizing all leaves and calculating the area in ImageJ software (Schneider *et al.*, 2012). Specific leaf area (SLA, $cm^2\ g^{-1}$) was calculated as the ratio between leaf area and leaf dry weight. The 5^{th} phytomer from bottom to top was collected for anatomical analysis (Fig. 2B).

For leaf development analysis, leaf primordia (≤ 1 cm), young (≤ 2 cm) and expanding (≤ 3 cm) leaves were sampled from seedlings 20 days after germination (DAG) (Fig. 2C).

For floral meristem differentiation analysis, seeds were sown in vermiculite, left for four days in the darkness to synchronize germination and apex meristem dissected under magnifying glass 4, 6, 8, 12 and 15 DAG. The meristems were classified according to their morphology (Fig. 3B). The corresponding cotyledons were pooled, frozen in liquid nitrogen and stored at -80°C for further analysis (Fig. 3C). Twenty-five seedlings were analyzed for each sampling point.

For flowering time, yield and fruit quality analysis, two sets of 12 plants per genotype (destructive and non-destructive) were grown for 120 days. Flowering time was measured in both sets (Fig. 3A). The destructive set was used to sample fully expanded leaves (5^{th} phytomer from bottom to top) and fruit pericarp at mature green (MG, when the placenta displays a gelatinous aspect, approximately 33 days post-anthesis); breaker (Br, when the first signal of carotenoids accumulation is observed, approximately 36 days post-anthesis); breaker + N (BrN, N days after breaker). Five biological replicates were sampled, each one composed of leaves or fruits from at least four plants. The non-destructive set was used for yield evaluation (Fig. 3D). Total number of flowers and fruits, total fresh weight of fruits and vegetative aerial fresh and dry weight were recorded. Harvest index was calculated according to the formula:

HI = (total fruit fresh weight)/(total vegetative aerial fresh weight + total fruit fresh weight).

Anatomical analysis

For leaf anatomical analysis, a fragment (1 × 0.5 cm) of the terminal leaflets from fully expanded leaves (5^{th} phytomer from bottom to top) was excised and fixed in FAA70 (formalin-acetic acid-ethanol 70%, 1:1:18) 24 h under vacuum (500 mmHg). Subsequently, the samples were dehydrated in ethanol series (10%, 30%, 70%, 80%, 90% and 95%, v/v) under vacuum (500 mm Hg). Pre-infiltration was performed with resin and ethanol 95% (1:1) with daily 2 h under vacuum (500 mm Hg) for one week, and infiltration was done in resin under the same conditions. Cross-

sections of 5 μm thickness were mounted on blades and stained with 0.05% toluidine blue. The images were captured in a light microscope (Zeiss AxioScope A1, Jena, Germany) and analyzed in the ImageJ software (Schneider *et al.*, 2012).

IAA quantification

The endogenous 3-Indoleacetic acid (IAA) was extracted and quantified as described by Silveira *et al.* (2004). Briefly, 150 mg of powdered tissue was homogenized in 2.5 mL of the extraction buffer containing 80% (v/v) ethanol, 1% (w/v) polyvinylpyrrolidone-40 and 0.05 μCi [3H]IAA, used as an internal standard. Samples were incubated and subsequently centrifuged. The supernatant was collected and the extraction was repeated once. The combined supernatants were completely vacuum-dried, redissolved in 90 μL of 10% methanol/0.5% acetic acid and filtered through a 0.2-μm membrane. IAA levels were determined by high-performance liquid chromatography (HPLC) in a 5 μm C18 column (Shimadzu Shin-pack CLC ODS) with a fluorescence detector (excitation at 280 nm, emission at 350 nm). Fractions containing IAA were collected and analyzed in a scintillation counter (Packard Tri-Carb) to estimate losses during the procedure. IAA quantification was performed based on a standard curve.

Fruit colorimetric measurement

Fruit surface color was determined at the equator of each collected fruit using a colorimeter (Konica Minolta, CR-400, 8-mm aperture, D65 illuminant, United States). Three measurements were taken at the equator of each fruit and average values were calculated as described in Cruz *et al.* (2018).

Carotenoids extraction, identification and quantification

Fruit carotenoid extraction was performed according to Sérino *et al.* (2009) with modifications. Aliquots of 200 mg fresh weight (FW) of fruit samples were sequentially extracted with NaCl saturated solution and dichloromethane and hexane:diethyl ether (1:1 v/v). After centrifugation, the supernatant was collected, and the hexane:diethyl ether extraction was repeated three more times. All supernatants were combined, and samples were dried by vacuum and dissolved in 200 μL of acetonitrile. Chromatography was carried out on a HPLC-DAD (model: 1260 system, Agilent Technologies, USA) equipped with an autosampler using a Phenomenex Luna C18 column (250 x 4.6 mm; 5 μm particle diameter) at room temperature with a flow rate of 0.8 mL min^{-1} and injection volume of 20 μL. The chromatographic method was constituted by a gradient of mixtures of solvents A (ethyl acetate) and B (acetonitrile:water 9:1 v:v) of 0-4 min with 0-5% B; 4-12 min with 5-10% B; 12-17 min with 10-20% B; 17-20 min with 20-65% B; 20-35 min with 65% B; 35-40 min with 65-0% B. Eluted compounds were detected between 340-700 nm

and quantified at 450 nm. Identification and quantification were determined with a calibration curve using commercial standards.

Phenolics extraction, identification and quantification

For phenolic content analysis, approximately 200 mg FW of fruit pericarp samples were extracted with 1 mL of 80% methanol (v:v) for 30 min in an ultrasonic bath at room temperature followed by the collection of the supernatants by centrifugation (13000 g, 4 min, 25°C). Phenolic compounds were analyzed by the HPLC-DAD (model: 1260 system, Agilent Technologies, USA) equipped with an autosampler, using a Zorbax Eclipse Plus C18 column (150 x 4.6 mm, 3.5 µm particle diameter) at 45ºC with a flow rate of 1 mL min^{-1} and injection volume of 3 µL. The chromatographic method was constituted by a gradient of mixtures of solvents A (0.1 % acetic acid in water) and B (acetonitrile) of 0-6 min with 10% B; 6-7 min with 10-15% B; 7-22 min with 15% B; 22-23 min with 15-20% B; 23-33 min with 20% B; 33-34 min with 20-25% B; 34-44 min with 25% B; 44-54 min with 25-50% B; 54-60 min with 50-100% B. Identification of metabolites was carried out through commercial or previously isolated components and quantification was determined with a calibration curve using commercial rutin standard.

Promoter analyses

For motif identification in *SlPIF4*, *SlBBX20*, *SlCHS1*, *SlCHI*, *SlF3H*, *SlFLS* promoters, 2000 bp upstream the ATG start codon were retrieved from the Sol Genomics Network (https://solgenomics.net). Using PlantPan 3.0 platform (Chow *et al.*, 2019), the following motifs were surveyed in the sequences: for BBXs: CCAAT (Ben-Naim *et al.*, 2006), CORE2 ($TGTGN_{2-3}$ATG, Tiwari *et al.*, 2010), CCACA (Gnesutta *et al.*, 2017), G-box (CACGTG, Song *et al.*, 2020) and modified G-box (TACGTG, Xiong *et al.*, 2019); for PIFs: PBE-box(CACATG, Zhang *et al.*, 2013),G-box (CACGTG, Toledo-Ortiz *et al.*, 2014) and E-box (CANNTG, Zhang *et al*., 2013); for RIN: C[CT][AT][AT][AT][AT][AT][AT][AG]G (Bianchetti *et al*., 2022), modified CArG (C[ACT][AT][AT][AT][AT][AT][AT][ATG]G, Fujisawa *et al*., 2013) and; for HY5: ACE-box (ACGT, Wang *et al.*, 2021).

Glycoalkaloids extraction, identification and quantification

Fruit pericarps at Br10 from WT and *slbbx20* plants were harvested and snap-frozen in liquid nitrogen. Metabolite extraction was performed on 50 mg of powdered tissue using 1 mL of 80% methanol (v/v). Samples were centrifugated and the supernatant was vacuum-drying. The pellets were resuspended in 100 uL of MilliQ water. Samples were subjected to Ultra Performance Liquid Chromatography High Resolution Mass Spectrometry (UPLC-HRMS) at the VIB Metabolomics Core Ghent (https://metabolomicscore-gent.sites.vib.be/en). Aliquots of 10 uL were injected on a Waters Acquity UHPLC (Waters) device connected to a Vion HDMS Q-TOF mass spectrometer

(Waters). Chromatographic separation was carried out on an ACQUITY UPLC BEH C18 (150 x 2.1 mm; 1.7 µm) column (Waters), column temperature was maintained at 40 °C. A gradient of two buffers was used for separation: buffer A (water + 0.1% formic acid, pH 3) and buffer B (acetonitrile + 0.1% formic acid, pH 3), as follows: 99 % A decreased to 50% A in 30 min, decreased to 30% from 30 to 35 minutes, and decreased to 0% from 35 to 37 minutes. The flow rate was set to 0.35 mL/min. Electrospray Ionization (ESI) was applied, LockSpray ion source was operated in positive ionization mode under the following specific conditions: capillary voltage, 2.5 kV; reference capillary voltage, 2.5 kV; source temperature, 120 °C; desolvation gas temperature, 550 °C; desolvation gas flow, 800 L/h; and cone gas flow, 50 L/h. The collision energy for full MS scan was set at 4 eV for low energy settings, for high energy settings (HDMSe) it was ramped from 20 to 70 eV. For DDA-MSMS the low mass ramp was ramped between 15-50 eV, and the high mass ramp was ramped between 50-120 eV. Mass range was set from 50 to 1500 Da, scan time was set at 0.1 s. Nitrogen (greater than 99.5%) was employed as desolvation and cone gas. Leucine-enkephalin (100 pg/µL solubilized in water:acetonitrile 1:1 [v/v], with 0.1% formic acid) was used for the lock mass calibration, with scanning every 2 min at a scan time of 0.1 s. Profile data was recorded through Unifi Workstation v2.0 (Waters). Data processing was performed with Progenesis QI software version 3.0 (Waters) for chromatogram alignment and compound ion detection. The detection limit was set at medium sensitivity with a minimum peak width of 0.03 min. Data is normalized to dry weight. In ESI+ ionization, 17475 compound ions were detected and aligned to a "pooled sample". Identification of steroidal glycoalkaloids (SGAs) was performed by analyzing a tomatine standard (Tomatine, #0602, Extrasynthese, France) and comparing the MS and MS/MS fragments.

***Botrytis cinerea* inoculation assay**

Botrytis cinerea (strain B05) was grown and maintained on potato dextrose agar media (1.5% agar, 2% potato extract, 2% dextrose). Conidia were collected from agar plates with distilled water and a glass rod, filtered and resuspended in a 0.1 M sucrose/0.07 M KH_2PO_4 solution to induce germination (Elad, 1991).

Fruits at Br4 stage were inoculated as described by Cantu *et al.* (2009). Briefly, on the day of harvest, tomato fruits were disinfected by 10% (v/v) bleach followed by three water rinses. Fruits were punctured (2 mm depth, 1 mm diameter) at seven sites. Six sites were inoculated with 10 µL of conidia suspension (3000 spores μL^{-1}), and the seventh was inoculated with 10 µL of sterile water as control. Fruits were incubated for 2 days at 24°C in a dark and damp environment. Lesion areas were measured on digital photographs using ImageJ software (Schneider *et al.*, 2012). Susceptibility was determined daily as disease incidence (percentage inoculation sites showing symptoms of tissue maceration or soft rot) and severity (diameters of the lesions). The evaluation of susceptibility was repeated three times with 15 fruits per replicate.

Data analyses

Differences in parameters were analyzed in Infostat software version 17/06/2015 (Di Rienzo *et al.*, 2011). When the data set showed homoscedasticity, Student's t-test ($P \leq 0.05$) was performed to compare mutant plants against the control genotype. In the absence of homoscedasticity, a non-parametric comparison was performed by applying the Kruskal-Wallis test ($P \leq 0.05$). All values represent the mean of at least four biological replicates.

RESULTS

SlBBX20 characterization and generation of loss-of-function mutant

SlBBX20 (Solyc12g089240) encodes a protein of 329 amino acids with two B-box domains that belongs to the structure group IV of the BBX protein family (Lira *et al.*, 2020). The presence of nuclear localization signals (NLSs) was predicted with three different platforms. According to cNLS mapper, SlBBX20 protein has two nonclassical bipartite NLSs at the N-terminal portion and one classical type 2 NLS at the C-terminal end, suggesting nuclear and cytoplasmic localization (Supplementary Fig. S2A). However, DeepLoc 2.0 and BaCelLo predicted SlBBX20 exclusively as a nuclear protein (Supplementary Table S2). This result was validated by fusing the *SlBBX20* coding sequence to the green fluorescence protein (GFP). The transient expression of the fusion protein in *Nicotiana benthamiana* leaves confirmed that SlBBX20 is indeed targeted to the nucleus (Supplementary Fig. S2B). Additionally, SlBBX20 homodimerization was confirmed by bimolecular fluorescence complementation (BiFC) assay (Supplementary Fig. S2B).

To further investigate SlBBX20 function, a knockout mutant line was obtained by CRISPR-Cas9-mediated genome edition using two target guides (Supplementary Fig. S3A). *Slbbx20* mutant harbors a deletion of 967 bp and an insertion of 14 bp, generating a premature stop codon that results in a truncated protein of 28 amino acids without any recognizable domain (Supplementary Fig. S3A). *SlBBX20* mRNA level in the mutant was almost undetectable (Supplementary Fig. S3B), most likely due to mRNA nonsense-mediated decay triggered by the premature termination codon in the expressed transcript (Lykke-Andersen and Bennett, 2014).

SlBBX20 regulates seedling photomorphogenesis and shade avoidance response

As the canonical function of BBX proteins is associated with seedling photomorphogenesis, an experiment was performed to investigate *Slbbx20* seedling development under different light conditions. After four days of dark treatment, mutant hypocotyls showed no difference in length compared to wild-type (WT) counterparts (Fig. 1A). However, mutant seedlings had longer hypocotyls when maintained under constant white light (Fig. 1B). In *A. thaliana*, increased

hypocotyl growth under prolonged shade depends on *PHYTOCHROME INTERACTING FACTOR 4* (*PIF4*)-mediated auxin signaling, but does not rely on maintaining elevated auxin biosynthetic rates in the cotyledon (Pucciariello *et al.*, 2018). In fact, the expression of the auxin biosynthetic genes reduces after several hours of exposure to low red/far-red (R/FR) ratios (de Wit *et al.*, 2015). Persistent PIF4 activity is needed for hypocotyl elongation under prolonged shade because it induces *INDOLE-3-ACETIC ACID 19* (*IAA19*) and *IAA29* auxin signaling factors, which are repressors of *IAA17*, a major inhibitor of hypocotyl growth (Pucciariello *et al.*, 2018). In this context, to understand the mechanism underneath the observed phenotype, we examined auxin content by monitoring the mRNA levels of the biosynthetic genes in cotyledons. As observed in *A. thaliana*, the mRNA levels of the five tested genes did not indicate that altered auxin biosynthesis is behind the higher hypocotyl elongation observed in *Slbbx20* mutant (Supplementary Fig. S4). In contrast, analysis of *SlPIF4*-mediated auxin signaling in hypocotyl revealed the upregulation of *SlPIF4* and *SlIAA29*, while *SlIAA17* was downregulated in *Slbbx20* (Fig. 1C). To better understand the role of SlBBX20 in this transcriptional cascade, we first demonstrated the physical interaction between SlBBX20 and SlPIF4 by yeast-two hybrid (Y2H) and BiFC assays (Fig. 1D). In addition, transient expression assays (TEA) revealed that SlPIF4 induces its own promoter, while the presence of SlBBX20 diminishes this transcriptional activation (Fig. 1E). This agrees with that observed in *A. thaliana* where AtPIF4 binds its own promoter inducing its transcriptional activity (Lee *et al.*, 2021). Altogether, these results indicate that SlBBX20 is a positive regulator of photomorphogenesis and participates in light-mediated hypocotyl elongation inhibition through the negative control of SlPIF4 activity via heterodimerization.

To further investigate the light signaling impairment observed in *Slbbx20* mutant, we analyzed the shade avoidance response by exposing the tomato plants for 15 days under low R/FR ratio (Fig. 1F). As evidenced by the increased hypocotyl, first internode and plant height, WT plants triggered shade avoidance response (SAR) after low R/FR ratio treatment. On the contrary, *Slbbx20* mutant phenotype was similar to that observed for WT plants maintained in shade conditions regardless the light treatment. In line with this phenotype, the expression of the negative regulator of SAR, *SlPAR1*, was diminished in mutant leaves (Fig. 1G). Hence, these findings implicate SlBBX20 as a negative regulator of SAR in tomato.

SlBBX20 positively regulates vegetative growth

The functional characterization of *SlBBXs*, particularly *SlBBX17* and *SlBBX28*, identified these genes as regulators of vegetative growth (Xu *et al.*, 2022; Lira *et al.*, 2022). To address whether this is also the case for *SlBBX20*, the development of 55-day-old *Slbbx20* plants was examined by measuring biomass parameters. Mutant plants were shorter with reduced leaf number and area, resulting in diminished dry weight (Fig. 2A). Interestingly, the specific leaf area was higher in

Slbbx20 than in WT plants (Fig. 2A). To further dissect this phenotype, a morpho-anatomical analysis was performed. Mutant leaf lamina was thinner due to the reduced thickness of the adaxial epidermis and the palisade and spongy parenchyma without changes in the number of cell layers (Fig. 2B). However, in *Slbbx20* mutant leaves, the number of palisade parenchyma cell per length unit was higher than in WT counterparts (Fig. 2B).

The mechanism underneath the observed misregulation of cell division and/or expansion was investigated through a comprehensive transcriptional profile along leaf development (Fig. 2C and Supplementary Table S3). Auxins play a central role in controlling cell division and expansion (Perrot-Rechenmann, 2010; Gomes and Scortecci, 2021); therefore, its metabolism was investigated. In *Slbbx20* leaf primordia, the expression of auxin biosynthetic genes, *i.e. TRYPTOPHAN AMINOTRANSFERASE 1* (*SlTAR1*) and two *YUCCA-LIKE FLAVIN MONOOXYGENASES* (*SlYUC1* and *SlYUC2*), were upregulated in line with the observed increment in auxin content. Accordingly, cell division-related genes, *i.e. CYCLIN-DEPENDENT KINASE-B2* (*SlCDKB2*) and three *CYCLIN*s (*SlCYCB1*, *SlCYCB2* and *SlCYCD3*), were also induced in the *Slbbx20* mutant (Fig. 2C and Supplementary Table S3). In contrast, *EXPANSIN-A5* (*SlEXPA5*), the most abundantly *SlEXP* expressed in leaves according to TomExpress (Zouine *et al.*, 2017), was downregulated in young and expanding *Slbbx20* leaves.

Collectively, this data indicate that SlBBX20 regulates auxin metabolism, ensuring the proper cell division and expansion rate, and playing a positive role in controlling vegetative growth.

Loss of *SlBBX20* disturbs flowering and yield

Flowering is known to be regulated by BBX proteins since the first functional characterization of a member of this family. AtBBX1, also known as CONSTANS (AtCO, Putterill *et al.*, 1995), is an inductor of the florigen *FLOWERING LOCUS T* (*AtFT*). Once synthesized in leaves, AtFT protein is translocated to the shoot apex, where induces meristem transition from vegetative to floral (An *et al.*, 2004). Hitherto, several other BBXs were identified as positive or negative regulators of flowering (Cao *et al.*, 2023). Thus, we examined whether SlBBX20 plays a role in tomato flowering. *Slbbx20* plants delayed the first anthesis without increasing the number of leaves (Fig. 3A). Then, we monitored the meristem transition in WT and *Slbbx20* seedlings (Fig. 3B). Both genotypes had the apical meristem in the vegetative stage at 4 days after germination (DAG). While the meristem transition began 6 DAG in WT seedlings, this only occurred 8 DAG in *Slbbx20* seedlings. Even 15 DAG, when all WT meristems were either in the transition or floral stage, some *Slbbx20* meristems were still vegetative. The transcriptional profile of *SlSFT* in the cotyledons explained this delay since its transcripts peak shifted from 4 DAG in WT to 8 DAG in *Slbbx20* seedlings (Fig. 3C).

Given the developmental delay observed, we investigated the effect of SlBBX20 deficiency on plant yield. After cultivation for 120 days, the number of flowers produced by the mutant was 50

% lower than in WT plants resulting in fewer fruits per plant (Fig. 3D). Ultimately, as both total fruit and shoot weight were reduced, the harvest index of the *Slbbx20* plants did not differ from WT genotype (Fig. 3D). These results suggest that mutant plants have a general delay in development rather than a direct regulation of flowering time.

Altogether, the data presented unveil SlBBX20 as pivotal factor in vegetative and reproductive development.

SlBBX20 expression is induced by the fruit ripening regulator SlRIN

SlBBX20 mRNA levels have been shown to increase during fruit ripening (Supplementary Fig. S1) and SlRIN, a master ripening regulator TF, binds to *SlBBX20* promoter (Lira *et al.*, 2020), suggesting that SlRIN induces *SlBBX20* transcription. To further investigate this relationship, *SlBBX20* transcripts were profiled in *Slrin* mutant fruits. At mature green (MG) stage, no differences were detected between genotypes. With the onset of ripening, *SlBBX20* transcript amount rapidly accumulated from MG to breaker (Br), remaining constant until the fully ripe stage (Br10) in WT fruits. However, *Slrin* mutant fruits displayed reduced levels of *SlBBX20* mRNA compared to WT counterparts (Fig. 4A). On the contrary, *SlRIN* transcripts were unaltered in *Slbbx20* fruits (Supplementary Fig. S5).

BBX (Cao *et al.*, 2023) and SlRIN TFs (Bemer *et al.*, 2012) are known to heterodimerize with other regulatory factors, thus, the putative interaction between SlBBX20 and SlRIN was tested and confirmed by BiFC assay and Y2H (Fig. 4B). Additionally, not only SlRIN binds *SlBBX20* promoter (Lira et al. 2020), but also BBX putative binding motifs were found in the promoter of *SlBBX20*. Therefore, we performed a TEA to better understand the ripening-related transcriptional regulation of this gene and the biological significance of SlRIN-SlBBX20 interaction (Fig. 4C). Either SlRIN or SlBBX20 alone induced the *SlBBX20* gene promoter in approximately 30% of the basal activity. Interestingly, the presence of both TFs together resulted in an over-induction of *SlBBX20* promoter, increasing in 170% the fLUC/rLUC ratio. These results unveiled that *SlBBX20* ripening-associated expression is triggered by the combined activity of SlRIN and SlBBX20.

SlBBX20 positively regulates fruit flavonoid accumulation

Slbbx20 fruits displayed a visual orangish color, which was confirmed by a higher Hue angle compared to WT counterparts (Supplementary Fig. S6). In tomato, two classes of specialized metabolites are responsible for fruit pigmentation, carotenoids and flavonoids (Dhar *et al.*, 2015). Surprisingly, only punctual differences in phytoene and phytofluene, which are colorless carotenoids, were detected in *Slbbx20* fruits, without altering the total carotenoid content (Supplementary Table S4). On the contrary, the three classes of flavonoids (*i.e.* naringenin

chalcone, kaempferol and quercetin derivatives) were dramatically reduced in mutant fruits, especially at the fully ripe stage (Br10, Fig. 5 and Supplementary Table S5).

To understand how SlBBX20 regulates flavonoid accumulation, we profiled the mRNA amount of the following biosynthetic genes: *CHALCONE SYNTHASE* (*SlCHS1* and 2), *CHALCONE ISOMERASE* (*SlCHI*), *FLAVANONE 3-HYDROXYLASE* (*SlF3H*), *FLAVANONE 3'-HYDROXYLASE* (*SlF3'H*) and *FLAVONOL SYNTHASE (SlFLS).* In the case of *SlCHI* that have six paralogs, the only one expressed in fruits according to TomExpress (Zouine *et al.*, 2017) was selected. In line with the flavonoid content, with the exception of *SlCHS2* that was unaltered (Supplementary Table S6), the tested genes were strongly downregulated along the ripening of mutant fruits (Fig. 5).

In tomato seedlings, the expression of flavonoid biosynthetic genes was induced by SlBBX25 overexpression, leading to anthocyanin accumulation (Luo *et al.*, 2021). Moreover, the lack of SlHY5 resulted in the reduction of fruit flavonoids content, as well as the downregulation of the corresponding biosynthetic genes and *SlBBX20* mRNA levels (Wang *et al.*, 2021). In this context, our results led to the hypothesis that SlBBX20 plays a role in SlHY5-mediated flavonoid induction. Interestingly, the physical interaction between SlBBX20 and SlHY5 was previously reported by Yang et al. (2022) and confirmed here by Y2H assay (Fig. 6A). Furthermore, the transcriptional induction of *SlBBX20* by SlHY5 was demonstrated by TEA (Fig. 6B). Through an *in silico* analysis, putative binding motifs for both these proteins were found in the promoter of *SlCHS1*, *SlCHI*, *SlF3H* and *SlFLS*. Then, a TEA was performed with SlBBX20 and/or SlHY5 as effectors (Fig. 6C). While SlBBX20 activated up to four times the tested promoters and SlHY5 had little to no effect on their transcriptional activity, the presence of both effectors dramatically induced up to 10 times the basal fLUC/rLUC ratio.

These results indicated that SlBBX20 induces flavonoid accumulation in fruits by upregulating the transcription of the biosynthetic genes through the heterodimerization with SlHY5.

Loss of *SlBBX20* decreases the accumulation of steroidal glycoalkaloids in tomato fruit

It has been previously shown that SlHY5 also regulates steroidal glycoalkaloids (SGAs) production in tomato, by directly binding to biosynthetic gene promoters (Wang *et al.*, 2018). Based on this information and the interaction between SlHY5 and SlBBX20, demonstrated above, we investigated whether SGAs accumulation is affected by loss of SlBBX20 in fully ripe (Br10) fruits. To this end, we performed targeted metabolomics in fully ripe tomato fruit from WT and mutant plants. We observed a decrease in the levels of α-tomatine and dehydrotomatine, as well as in SGAs downstream of α-tomatine (*i.e.* putative acetoxytomatine, hydroxytomatine and esculeoside) (Supplementary Table S7).

SlBBX20 attenuates *Botrytis cinerea* infection

Common factors between light and defense signaling transduction pathways have been reported (Pierik and Ballaré, 2021). Moreover, flavonoids are important nutraceutical compounds with antioxidant activity that play a major role in postharvest disease resistance (Hoensch and Oertel, 2015). Indeed, high concentrations of these compounds in fruits often correlate with low incidence of pathogens (Treutter, 2006). Tomatine also plays an important role in biotic defense, and the ability of the pathogen to deactivate this compound determines the success of infection (Sandrok and VanEtten, 1998; Pareja-Jaime *et al.*, 2008; Ito *et al.*, 2007; Dahlin *et al.*, 2017). Due to the above demonstrated effect of SlBBX20 on flavonoids and SGAs accumulation, *Slbbx20* fully ripe fruits were inoculated with the necrotrophic fungus *Botrytis cinerea*. The number of infected inoculated sites and the lesion area were higher in *Slbbx20* than in WT fruits 48 h post-infection (Fig. 7).

DISCUSSION

Knowledge of *BBX* gene family has greatly increased in recent years unveiling BBX proteins as regulatory factors that play pleiotropic functions in plant growth (Cao *et al.*, 2023). Consequently, their study in crop species is particularly interesting since by affecting different stages of plant development, BBXs can modulate agronomical important traits, such as harvestable organs yield and quality (Shalmani *et al.*, 2023). In this sense, here, we functionally characterized tomato *SlBBX20* (Solyc12g089240), which codifies a BBX protein with two B-box domains and whose transcription is abruptly upregulated upon fruit ripening in a phytochrome-mediated manner (Lira *et al.*, 2020).

The behavior of *Slbbx20* mutant in response to distinct growth conditions demonstrated that SlBBX20 is a positive regulator of light signaling, reinforcing its previously described role as a downstream factor in phytochrome-mediated signaling cascade (Lira *et al.*, 2020). Our data showed that SlBBX20 participates in light-mediated growth inhibition through the heterodimerization with SlPIF4 that, in turn, negatively regulates SlPIF4 activity and, consequently, the downstream auxin signaling cascade (*i.e, SlIAA29* and *SlIAA17*). In the absence of SlBBX20, mutant plants are hyposensitive to light, maintaining higher PIF4-mediated crosstalk between light and auxin signaling, as observed in *A. thaliana* under prolonged shade (Pucciariello *et al.*, 2018). In agreement with this regulatory mechanism, the physical interaction between AtPIF4 and AtBBX11 inhibits AtPIF4-mediated *AtIAA29* transcriptional induction (Song *et al.*, 2021).

Plants have two strategies to deal with shade: shade tolerance and shade avoidance. Shade-tolerant species are adapted to the understory of tree canopies (Gommers *et al.*, 2013). Differently, shade avoidance is induced by low photosynthetically active radiation and low R/FR ratio and, in this case, plants maximize light capture by increasing stem length and positioning the leaves out of

the shade via photoreceptor signaling networks (Fernández-Milmanda and Ballaré, 2021). Several reports have investigated the effect of prolonged shade on growth and phenology of shade-avoiding plants. *A. thaliana* plants grown under constant shade developed fewer leaves with reduced area due to attenuated leaf initiation and cell expansion rate, respectively (Cookson and Granier, 2006). Further experiments showed that while energy signals mediated by TARGET OF RAPAMYCIN kinase pathway are sufficient to stimulate cell proliferation in shoot meristem even in the dark, the development of a normal leaf lamina requires photomorphogenesis-like hormonal responses (Mohammed *et al.*, 2018). Similar results have been observed in soybean, as plants grown under shade conditions showed decreased leaf size caused by the differential expression of cell proliferation and/or expansion genes dependent on the leaf developmental stage (Wu *et al.*, 2017). Similarly, *Slbbx20* plants displayed a misregulation of these processes. Although mutant leaves contained more cells due to an increased expression of cell division-related genes preceded by a peak in auxin biosynthesis at leaf primordia stage; cell size was compromised by the reduced amount of *SlEXPA5* mRNA in expanding leaves, resulting in plants with diminished size. Shade also delays flowering and compromises yield in strawberry (Takeda *et al.*, 2010) and soybean (Cober and Voldeng, 2001; Kurosaki and Yumoto, 2003), as observed in *Slbbx20* mutant. Concluding, SlBBX20 deficiency phenocopies plants growing under shade conditions displaying a seemingly constitutive SAR, which delays vegetative and reproductive growth resulting in smaller plants with reduced yield.

Recent reports have shown a key role of BBX proteins as inductors of specialized metabolism in tomato fruits. SlBBX25 (Solyc01g110180) is a positive regulator of carotenoids (Xiong *et al.*, 2019) and anthocyanins (Luo *et al.*, 2021) accumulation through the direct interaction with the promoters of biosynthetic genes. Interestingly, both these pathways were strongly downregulated in *Slhy5* mutant fruits. Although SlHY5 binds to the promoter of carotenoid and flavonoid biosynthetic genes (Wang *et al.*, 2021), no information was available regarding its direct effect on their transcriptional activation until now. In this sense, our data unravel a flavonoid accumulation mechanism in which SlBBX20 (Solyc12g089240) induces the expression of the biosynthetic genes that is synergistically enhanced by the presence of SlHY5. Moreover, SlHY5 itself can induce the transcriptional activity of *SlBBX20* promoter, but not of flavonoids biosynthetic genes. Therefore, the previously reported flavonoid reduction in *Slhy5* mutant fruits is likely due to the downregulation of *SlBBX20* (Wang *et al.*, 2021). Such mechanism seems to be conserved in other species where the heterodimerization of BBXs and HY5 promotes flavonoids and anthocyanins accumulation, as described in *A. thaliana* (Bursch *et al.*, 2020) and *Pyrus pyrifolia* (Bai *et al.*, 2019)

The SGAs reduction in *Slbbx20* ripe fruits also corroborates the synergistic interaction model between SlHY5 and BBX20 for the regulation of fruit metabolism. SGAs levels were decreased but not abolished by the absence of SlBBX20. Similarly, loss of SlHY5 produced analogous

effects to SGAs accumulation (Zhang *et al.*, 2022). This evidence indicates that SlHY5 interacts with BBX20 to modulate the expression of the SGAs pathway.

The antifungal effect of flavonoids has been extensively reported *in planta* and, in fruits and vegetables postharvest resistance (Treutter, 2006). *Pyricularia oryzae* growth is inhibited by naringenin, kaempferol and quercetin in decreasing order (Padmavati *et al.*, 1997). Protoanthocyanidins and dihydroquercetin are involved in barley resistance to *Fusarium* species (Skadhauge *et al.*, 1997), while quercetin and its derivatives inhibit *Neurospora crassa* growth (Parvez *et al.*, 2004). Besides, JA-mediated SGAs accumulation is known to repress fungal infection in tomato (Montero-Vargas *et al.*, 2018). It is known that light-mediated plant growth and defense response crosstalk in an intricate network (Pierik and Ballaré, 2021). In a direct way, low R/FR ratios suppress the formation of jasmonyl-L-isoleucine (JA-Ile), the bioactive conjugate of the defense hormone jasmonic acid (JA). This mechanism involves the PIF-mediated activation of a JA-catalyzing enzyme resulting in the enhanced stability of JASMONATE-ZIM DOMAIN (JAZ) proteins and reduced defense response (Fernández-Milmanda *et al.*, 2020). In this context, although the exact function of SlBBX20 in the regulation of specialized metabolism and fruit defense must be further investigated, the susceptibility to *B. cinerea* observed in *Slbbx20* fruits might be partially due to reduced flavonoids and SGAs content, as well as possibly alterations in JA production and signaling.

Altogether, the obtained data revealed SlBBX20 is a positive regulator of light signaling that controls growth by limiting SlPIF4 activity. Afterwards, in an auxin-related manner, SlBBX20 coordinates cell division and expansion, ensuring normal growth rate and, consequently, vegetative and reproductive development. Finally, the accumulation of SlBBX20 during ripening in response to SlRIN, enhances fruit flavonoid content by the direct induction of the biosynthetic genes, which is boosted by SlBBX20-SlHY5 interaction. In summary, this work provides further evidence that manipulating BBXs is a suitable strategy for tailoring harvestable organ yield and quality (Fig. 8).

SUPPLEMENTARY DATA

The following supplementary data available at JXB online.

Supplementary Table S1. Primers used in the experiments

Supplementary Table S2. Nuclear localization signals (NLSs) predicted in SlBBX20 sequence

Supplementary Table S3. Relative transcript expression of cell division- and expansion-related genes in *Slbbx20* along leaf development

Supplementary Table S4. Carotenoids content in *Slbbx20* fruits

Supplementary Table S5. Flavonoids content in *Slbbx20* fruits

Supplementary Table S6. Relative transcript expression of flavonoid biosynthetic genes in *Slbbx20* fruits

Supplementary Table S7. Steroidal glycoalkaloids content in *Slbbx20* fruits

Supplementary Fig. S1. *SlBBXs* expression along fruit development

Supplementary Fig. S2. SlBBX20 protein characterization

Supplementary Fig. S3. Characterization of *Slbbx20* mutant

Supplementary Fig. S4. *Slbbx20* seedling response to light

Supplementary Fig. S5. *SlRIN* expression in *Slbbx20* fruits

Supplementary Fig. S6. Ripe fruits of the *Slbbx20* mutant show orangish color

ACKNOWLEDGMENTS

We thank Silvia Blanco and Amanda Ferreira Macedo for the technical support.

AUTHOR CONTRIBUTIONS

Lumi Shiose, Juliene dos Reis Moreira and Bruno Silvestre Lira performed most of the experiments and analyzed the data; Maria José Oliveira, Raquel Tsu Ay Wu, Gabriel Ponciano Carvalho Souza, José Laurindo dos Santos Júnior, Eny Floh, Marcelo José Pena Ferreira and Gabriel Gomez Ocampo performed some experiments; Elke Clicque and Nikolaos Ntelkis performed the SGAs metabolite profiling experiment and analysis; Alain Goossens, Javier Botto, Luciano Freschi and Magdalena Rossi conceived the project, designed the experiments; Lumi Shiose, Juliene dos Reis Moreira, Bruno Silvestre Lira and Magdalena Rossi wrote the paper and collected the contributions of all authors. All authors read and approved the final manuscript. Magdalena Rossi agrees to serve as the author responsible for contact and ensures communication.

CONFLICTS OF INTEREST

The authors declare no conflict of interest.

FUNDING

LS, JRM, RTAW and GP were recipients of FAPESP (Fundação de Amparo à Pesquisa do Estado de São Paulo, Brazil) fellowships. MJO, MJPF, LF and MR were funded by fellowships from CNPq (Conselho Nacional de Desenvolvimento Científico e Tecnológico, Brasil). JLSJ was recipient of CAPES (Coordenação de Aperfeiçoamento de Pessoal de Nível Superior, Brazil) fellowship. BSL was recipient of a fellowship granted by GALY Company. This work was partially supported by grants from FAPESP 2016/01128-9 and 2021/0507-1 (Brazil), CAPES Finance Code 001 and USP (Brazil), the Research Foundation Flanders (grants G0F6220N and G0E1122N) and the European Union's Horizon 2020 Research and Innovation Program under Grant Agreement no 825730 (Endoscape).

DATA AVAILABILITY

All primary data that support the findings of this work are openly available upon request.

REFERENCES

An H, Roussot C, Suárez-López P, Corbesier L, Vincent C, Piñeiro M, Hepworth S, Mouradov A, Justin S, Turnbull C, Coupland G. 2004. CONSTANS acts in the phloem to regulate a systemic signal that induces photoperiodic flowering of *Arabidopsis*. Development **131**, 3615-3626.

Bai S, Tao R, Tang Y, Yin L, Ma Y, Ni J, Yan X, Yang Q, Wu Z, Zeng Y, Teng Y. 2019. BBX16, a B-box protein, positively regulates light-induced anthocyanin accumulation by activating *MYB10* in red pear. Plant Biotechnology Journal **17**, 1985-1997.

Bemer M, Karlova R, Ballester AR, Tikunov YM, Bovy AG, Wolters-Arts M, de Barros Rossetto P, Angenent GC, de Maagd RA. 2012. The tomato FRUITFULL homologs TDR4/FUL1 and MBP7/FUL2 regulate ethylene-independent aspects of fruit ripening. The Plant Cell **24**, 4437-4451.

Ben-Naim O, Eshed R, Parnis A, Teper-Bamnolker P, Shalit A, Coupland G, Samach A, Lifschitz E. 2006. The CCAAT binding factor can mediate interactions between CONSTANS-like proteins and DNA. The Plant Journal **46**, 462-476.

Bursch K, Toledo-Ortiz G, Pireyre M, Lohr M, Braatz C, Johansson H 2020. Identification of BBX proteins as rate-limiting cofactors of HY5. Nature Plants **6**, 921-928.

Cantu D, Blanco-Ulate B, Yang L, Labavitch JM, Bennett AB, Powell AL. 2009. Ripening-regulated susceptibility of tomato fruit to *Botrytis cinerea* requires *NOR* but not *RIN* or ethylene. Plant Physiology **150**, 1434-1449.

Cao J, Yuan J, Zhang Y, Chen C, Zhang B, Shi X, Niu R, Lin F. 2023. Multi-layered roles of BBX proteins in plant growth and development. Stress Biology **3**, 1.

Cao Y, Han Y, Meng D, Li D, Jiao C, Jin Q, Lin Y, Cai Y. 2017. B-BOX genes: genome-wide identification, evolution and their contribution to pollen growth in pear (*Pyrus bretschneideri* Rehd.). BMC Plant Biology **17**, 1-12.

Cao Y, Meng D, Han Y, Chen T, Jiao C, Chen Y, Jin Q, Cai Y. 2019. Comparative analysis of B-BOX genes and their expression pattern analysis under various treatments in *Dendrobium officinale*. BMC Plant Biology **19**, 245.

Čermák T, Curtin SJ, Gil-Humanes J, Čegan R, Kono TJ, Konečná E, Belanto JJ, Starker CG, Mathre JW, Greenstein RL, Voytas DF. 2017. A multipurpose toolkit to enable advanced genome engineering in plants. The Plant Cell **29**, 1196-1217.

Chang Y, Sun H, Liu S, He Y, Zhao S, Wang J, Wang T, Zhang J, Gao J, Yang Q, Li M, Zhao X. 2023. Identification of BBX gene family and its function in the regulation of microtuber formation in yam. BMC Genomics **24**, 1-15.

Chow C, Lee TY, Hung YC, Guan-Zhen L, Tseng KC, Liu YH, Kuo PL, Zheng HQ, Chang WC 2019. PlantPAN3.0: a new and updated resource for reconstructing transcriptional regulatory networks from ChIP-seq experiments in plants. Nucleic Acids Research **47**, D1155-D1163.

Chu Z, Wang X, Li Y, Yu H, Li J, Lu Y, Li H, Ouyang B. 2016. Genomic organization, phylogenetic and expression analysis of the B-BOX gene family in tomato. Frontiers in plant science **7**, 1552.

Cober ER, Voldeng HD 2001. Low R:FR light quality delays flowering of *E7E7* soybean lines. Crop Science **41**, 1823-1826.

Cookson SJ, Granier C. 2006. A dynamic analysis of the shade-induced plasticity in Arabidopsis thaliana rosette leaf development reveals new components of the shade-adaptative response. Annals of Botany **97**,.443-452.

Cruz AB, Bianchetti RE, Alves FRR, Purgatto E, Peres LEP, Rossi M, Freschi L. 2018. Light, ethylene and auxin signaling interaction regulates carotenoid biosynthesis during tomato fruit ripening. Frontiers in Plant Science **9**, 1370.

Cuéllar AP, Pauwels L, De Clercq R, Goossens A. 2013. Yeast two-hybrid analysis of jasmonate signaling proteins. Methods and Protocols. **1011**, 173-185.

Cui L, Zheng F, Wang J, Zhang C, Zhang D, Gao S, Zhang C, Ye J, Zhang Y, Ouyang B, Wang T, Hong Z, Ye Z, Zhang J. 2022. The tomato CONSTANS-LIKE protein SlCOL1 regulates fruit yield by repressing *SFT* gene expression. BMC Plant Biology **22**, 429.

Dahlin P, Müller MC, Ekengren S, McKee LS, Bulone V. 2017. The impact of steroidal glycoalkaloids on the physiology of Phytophthora infestans, the causative agent of potato late blight. Molecular plant-microbe interactions **30**, 531-542.

de Wit M, Ljung K, Fankhauser C. 2015. Contrasting growth responses in lamina and petiole during neighbor detection depend on differential auxin responsiveness rather than different auxin levels. New Phytologist **208**, 198-209.

Dhar MK, Sharma R, Koul A, Kaul S. 2015. Development of fruit color in Solanaceae: a story of two biosynthetic pathways. Briefings in Functional Genomics **14**, 199-212.

Di Rienzo JA. 2009. Statistical software for the analysis of experiments of functional genomics. RDNDA, Argentina

Di Rienzo JA, Casanoves F, Balzarini MG, Gonzalez L, Tablada M, Robledo YC. 2011. InfoStat versión 2011. Grupo InfoStat, FCA, Universidad Nacional de Córdoba, Argentina. http://www.infostat.com.ar **8**, 195-199.

Elad Y. 1991. An inhibitor of polyamine biosynthesis - Difluoromethylornithine - and the polyamine spermidine for the control of gray mold (*Botrytis cinerea*). Phytoparasitica **19**, 201-209.

Feng Z, Li M, Li Y, Yang X, Wei H, Fu X, Ma L, Lu J, Wang H, Yu S. 2021. Comprehensive identification and expression analysis of B-Box genes in cotton. BMC Genomics **22**, 1-16.

Fernández-Milmanda GL, Ballaré CL (2021). Shade avoidance: expanding the color and hormone palette. Trends in Plant Science **26**, 509-523.

Fernández-Milmanda GL, Crocco CD, Reichelt M, Mazza CA, Köllner TG, Zhang T, Cargnel MD, Lichy MZ, Fiorucci AS, Fankhauser C, Koo AJ, Austin AT, Gershenzon J, Ballaré CL. 2020. A light-dependent molecular link between competition cues and defence responses in plants. Nature Plants **6**, 223-230.

Gangappa SN, Botto JF 2014. The BBX family of plant transcription factors. Trends in Plant Science **19**, 460-470.

Gehl C, Waadt R, Kudla J, Mendel RR, Hänsch R. 2009. New GATEWAY vectors for high throughput analyses of protein-protein interactions by bimolecular fluorescence complementation. Molecular Plant **2**, 1051-1058.

Gnesutta N, Kumimoto RW, Swain S, Chiara M, Siriwardana C, Horner DS, Holt BF, Mantovani R. 2017. CONSTANS imparts DNA sequence specificity to the histone fold NF-YB/NF-YC dimer. The Plant Cell **29**, 1516-1532.

Gomes GLB, Scortecci KC 2021. Auxin and its role in plant development: structure, signalling, regulation and response mechanisms. Plant Biology **23**, 894-904.

Gommers CM, Visser EJ, St Onge KR, Voesenek LA, Pierik R. 2013. Shade tolerance: when growing tall is not an option. Trends in plant science **18**, 65-71.

Hoensch HP, Oertel R. 2015. The value of flavonoids for the human nutrition: Short review and perspectives. Clinical Nutrition Experimental **3**, 8-14.

Hou W, Ren L, Zhang Y, Sun H, Shi T, Gu Y, Wang A, Ma D, Li Z, Zhang L. 2021. Characterization of BBX family genes and their expression profiles under various stresses in the sweet potato wild ancestor Ipomoea trifida. Scientia Horticulturae **288**, 110374.

James P, Halladay J, Craig EA. 1996. Genomic libraries and a host strain designed for highly efficient two-hybrid selection in yeast. Genetics **144**, 1425-1436.

Jin H, Xing M, Cai C, Li S. 2019. B-box proteins in *Arachis duranensis*: genome-wide characterization and expression profiles analysis. Agronomy **10**, 23.

Karimi M, Inzé D, Depicker A. 2002. GATEWAY™ vectors for Agrobacterium-mediated plant transformation. Trends in Plant Science **7**, 193-195.

Kosugi S, Hasebe M, Matsumura N, Takashima H, Miyamoto-Sato E, Tomita M, Yanagawa H. 2009. Six classes of nuclear localization signals specific to different binding grooves of importin α. Journal of Biological Chemistry **284**, 478-485.

Kurosaki H, Yumoto S. 2003. Effects of low temperature and shading during flowering on the yield components in soybeans. Plant Production Science **6**, 17-23.

Lee S, Zhu L, Huq E. 2021. An autoregulatory negative feedback loop controls thermomorphogenesis in *Arabidopsis*. PLoS Genetics **17**, e1009595.

Lira BS, Oliveira MJ, Shiose L, Vicente MH, Souza GPC, Floh EIS, Purgatto E, Nogueira FTS, Freschi L, Rossi M. 2022. SlBBX28 positively regulates plant growth and flower number in an auxin-mediated manner in tomato. Plant Molecular Biology **110**, 253-268.

Lira BS, Oliveira MJ, Shiose L, Wu RTA, Rosado D, Lupi ACD, Freschi L, Rossi M. 2020. Light and ripening-regulated BBX protein-encoding genes in *Solanum lycopersicum*. Scientific Reports **10**, 19235.

Liu X, Li R, Dai Y, Chen X, Wang X. 2018. Genome-wide identification and expression analysis of the B-box gene family in the apple (*Malus domestica* Borkh.) genome. Molecular Genetics and Genomics **293**, 303-315.

Luo D, Sun W, Cai J, Hu G, Zhang D, Zhang X, Yang C, Ye Z, Wang T. 2023. SlBBX20 attenuates JA signalling and regulates resistance to *Botrytis cinerea* by inhibiting SlMED25 in tomato. Plant Biotechnology Journal **21**, 792-805.

Luo D, Xiong C, Lin A, Zhang C, Sun W, Zhang J, Yang C, Lu Y, Li H, Ye Z, He P, Wang T. 2021. SlBBX20 interacts with the COP9 signalosome subunit SlCSN5-2 to regulate anthocyanin biosynthesis by activating SlDFR expression in tomato. Horticulture Research **8**.

Lykke-Andersen J, Bennett EJ. 2014. Protecting the proteome: Eukaryotic cotranslational quality control pathways. Journal of Cell Biology **204**, 467-476.

Mohammed B, Bilooei SF, Dóczi R, Grove E, Railo S, Palme K, Ditengou FA, Bögre L, López-Juez E. 2018. Converging light, energy and hormonal signaling control meristem activity, leaf initiation, and growth. Plant Physiology **176**, 1365-1381.

Montero-Vargas JM, Casarrubias-Castillo K, Martínez-Gallardo N, Ordaz-Ortiz JJ, Délano-Frier JP, Winkler R. 2018. Modulation of steroidal glycoalkaloid biosynthesis in tomato (*Solanum lycopersicum*) by jasmonic acid. Plant Science **277**, 155-165.

Murashige T, Skoog F. 1962. A revised medium for rapid growth and bio assays with tobacco tissue cultures. Physiologia Plantarum **15**, 473-497.

Nguyen CV, Vrebalov JT, Gapper NE, Zheng Y, Zhong S, Fei Z, Giovannoni JJ. 2014. Tomato *GOLDEN2-LIKE* transcription factors reveal molecular gradients that function during fruit development and ripening. The Plant Cell **26**, 585-601.

Obel HO, Cheng C, Li Y, Tian Z, Njogu MK, Li J, Lou Q, Yu X, Yang Z, Ogweno JO, Chen J. 2022. Genome-wide identification of the B-Box gene family and expression analysis suggests their potential role in photoperiod-mediated β-carotene accumulation in the endocarp of cucumber (*Cucumis sativus* L.) fruit. Genes **13**, 658.

Padmavati M, Sakthivel N, Thara KV, Reddy AR. 1997 Differential sensitivity of rice pathogens to growth inhibition by flavonoids. Phytochemistry **46**, 499-502.

Pareja-Jaime Y, Roncero MIG, Ruiz-Roldán MC 2008. Tomatinase from Fusarium oxysporum f. sp. lycopersici is required for full virulence on tomato plants. Molecular plant-microbe interactions **21**, 728-736.

Parvez MM, Tomita-Yokotani K, Fujii Y, Konishi T, Iwashina T. 2004 Effects of quercetin and its seven derivatives on the growth of *Arabidopsis thaliana* and *Neurospora crassa*. Biochemical Systematics and Ecology **32**, 631-635.

Perrot-Rechenmann C. 2010. Cellular responses to auxin: division versus expansion. Cold Spring Harbor Perspectives in Biology **2**, a001446.

Pfaffl MW, Horgan GW, Dempfle L. 2002. Relative expression software tool (REST©) for group-wise comparison and statistical analysis of relative expression results in real-time PCR. Nucleic Acids Research **30**, e36.

Pierik R, Ballaré CL (2021). Control of plant growth and defense by photoreceptors: from mechanisms to opportunities in agriculture. Molecular Plant **14**, 61-76.

Pierleoni A, Martelli PL, Fariselli P, Casadio R. 2006. BaCelLo: a balanced subcellular localization predictor. Bioinformatics **22**, e408-e416.

Pino LE, Lombardi-Crestana S, Azevedo MS, Scotton DC, Borgo L, Quecini V, Figueira A, Peres LE. 2010. The *Rg1* allele as a valuable tool for genetic transformation of the tomato 'Micro-Tom' model system. Plant Methods **6**, 1-11.

Pucciariello O, Legris M. Rojas,CC, Iglesias MJ, Hernando CE, Dezar C, Vazquez M, Yanovsky MJ, Finlayson SA, Prat S, Casal JJ. 2018. Rewiring of auxin signaling under persistent shade. Proceedings of the National Academy of Sciences **115**, 5612-5617.

Putterill J, Robson F, Lee K, Simon R, Coupland G. 1995. The CONSTANS gene of *Arabidopsis* promotes flowering and encodes a protein showing similarities to zinc finger transcription factors. Cell **80**, 847-857.

Quadrana L, Almeida J, Otaiza SN, Duffy T, da Silva JVC, de Godoy F, Asís R, Bermúdez L, Fernie AR, Carrari F, Rossi M. 2013. Transcriptional regulation of tocopherol biosynthesis in tomato. Plant Molecular Biology **81**, 309-325.

Ruijter JM, Ramakers C, Hoogaars WMH, Karlen Y, Bakker O, Van den Hoff MJB, Moorman A. 2009. Amplification efficiency: linking baseline and bias in the analysis of quantitative PCR data. Nucleic Acids Research **37**, e45-e45.

Schneider CA, Rasband WS, Eliceiri KW. 2012. NIH Image to ImageJ: 25 years of image analysis. Nature Methods **9**, 671-675.

Shalmani A, Jing XQ, Shi Y, Muhammad I, Zhou MR, Wei XY, Chen QQ, Li WQ, Liu WT, Chen KM. 2019. Characterization of B-BOX gene family and their expression profiles under hormonal, abiotic and metal stresses in Poaceae plants. BMC Genomics **20**, 1-22.

Shalmani A, Ullah U, Tai L, Zhang R, Jing XQ, Muhammad I, Bhanbhro N, Liu WT, Li WQ, Chen KM. 2023. OsBBX19-OsBTB97/OsBBX11 module regulates spikelet development and yield production in rice. Plant Science **334**, 111779.

Shan B, Bao G, Shi T, Zhai L, Bian S, Li X. 2022. Genome-wide identification of BBX gene family and their expression patterns under salt stress in soybean. BMC Genomics **23**, 1-17.

Silveira V, Balbuena TS, Santa-Catarina C, Floh EI, Guerra MP, Handro W. 2004 Biochemical changes during seed development in *Pinus taeda* L. Plant Growth Regulation **44**, 147-156.

Skadhauge B, Thomsen K, von Wettstein D. 1997 The role of barley testa layer and its flavonoid content in resistance to *Fusarium* infections. Hereditas **126**, 147-160.

Song J, Lin R, Tang M, Wang L, Fan P, Xia X, Yu J, Zhou Y. 2023. SlMPK1- and SlMPK2-mediated SlBBX17 phosphorylation positively regulates CBF-dependent cold tolerance in tomato. New Phytologist **239**, 1887-1902.

Song K, Li B, Wu H, Sha Y, Qin L, Chen X, Liu Y, Tang H, Yang L. 2022. The Function of BBX Gene Family under Multiple Stresses in Nicotiana tabacum. Genes **13**, 1841.

Song Z, Heng Y, Bian Y, Xiao Y, Liu J, Zhao X, Jiang Y, Deng XW, Xu D. 2021. BBX11 promotes red light-mediated photomorphogenic development by modulating phyB-PIF4 signaling. Abiotech **2**, 117-130.

Song Z, Yan T, Liu J, Bian Y, Heng Y, Lin F, Jiang Y, Deng XW, Xu D. 2020. BBX28/BBX29, HY5 and BBX30/31 form a feedback loop to fine-tune photomorphogenic development. The Plant Journal **104**, 377-390.

Takeda F, Glenn DM, Callahan A, Slovin J, Stutte GW. 2010. Delaying flowering in short-day strawberry transplants with photoselective nets. International Journal of Fruit Science **10**, 134-142.

Talar U, Kiełbowicz-Matuk A. 2021. Beyond Arabidopsis: BBX regulators in crop plants. International Journal of Molecular Sciences 22, 2906.

Talar U, Kiełbowicz-Matuk A, Czarnecka J, Rorat T. 2017. Genome-wide survey of B-box proteins in potato (*Solanum tuberosum*) - Identification, characterization and expression patterns during diurnal cycle, etiolation and de-etiolation. PloS One **12**, e0177471.

Thumuluri V, Almagro-Armenteros JJ, Johansen AR, Nielsen H, Winther O. 2022. DeepLoc 2.0: multi-label subcellular localization prediction using protein language models. Nucleic acids research **50**, W228-W234.

Tiwari SB, Shen Y, Chang HC, Hou Y, Harris A, Ma SF, McPartland M, Hymus GJ, Adam L, Marion C, Belachew A, Repetti PP, Reuber TL, Ratcliffe OJ. 2010. The flowering time regulator CONSTANS is recruited to the *FLOWERING LOCUS T* promoter via a unique cis-element. New Phytologist. **187**, 57-66.

Treutter D. 2006. Significance of flavonoids in plant resistance: a review. Environmental Chemistry Letters **4**, 147-157.

Tripathi P, Carvallo M, Hamilton EE, Preuss S, Kay SA. 2017. *Arabidopsis* B-BOX32 interacts with CONSTANS-LIKE3 to regulate flowering. Proceedings of the National Academy of Sciences **114**, 172-177.

Vanden-Bossche, R, Demedts B, Vanderhaeghen R, Goossens A. 2013. Transient expression assays in tobacco protoplasts. Jasmonate Signaling: Methods and Protocols, 227-239.

Vrebalov J, Ruezinsky D, Padmanabhan V, White R, Medrano D, Drake R, Schuch W, Giovannoni J. 2002. A MADS-box gene necessary for fruit ripening at the tomato *Ripening-Inhibitor* (*Rin*) locus. Science **296**, 343-346.

Wang J, Yang G, Chen Y, Dai Y, Yuan Q, Shan Q, Pan L, Dai L, Zou X, Liu F, Xiong C. 2022. Genome-wide characterization and anthocyanin-related expression analysis of the *B-BOX* gene family in *Capsicum annuum* L. Frontiers in genetics **13**, 847328.

Wang W, Wang P, Li X, Wang Y, Tian S, Qin G. 2021. The transcription factor SlHY5 regulates the ripening of tomato fruit at both the transcriptional and translational levels. Horticulture Research **8**, 82.

Wang Y, Zhai Z, Sun Y, Feng C, Peng X, Zhang X, Xiao Y, Zhou X, Wang W, Jiao J, Li T. 2021a. Genome-wide identification of the B-BOX genes that respond to multiple ripening related signals in sweet cherry fruit. International Journal of Molecular Sciences **22**, 1622.

Wang Y, Zhang Y, Liu Q, Zhang T, Chong X, Yuan H. 2021b. Genome-Wide Identification and Expression Analysis of BBX Transcription Factors in *Iris germanica* L. International Journal of Molecular Sciences **22**, 8793.

Wang CC, Meng LH, Gao Y, Grierson D, Fu DQ 2018. Manipulation of light signal transduction factors as a means of modifying steroidal glycoalkaloids accumulation in tomato leaves. Frontiers in Plant Science **9**, 437.

Wei H, Wang P, Chen J, Li C, Wang Y, Yuan Y, Fang J, Leng X. 2020. Genome-wide identification and analysis of *B-BOX* gene family in grapevine reveal its potential functions in berry development. BMC Plant Biology **20**, 72.

Wu Y, Gong W, Yang W. 2017. Shade inhibits leaf size by controlling cell proliferation and enlargement in soybean. Scientific Reports **7**, 9259.

Wu Z, Fu D, Gao X, Zeng Q, Chen X, Wu J, Zhang N. 2023. Characterization and expression profiles of the B-box gene family during plant growth and under low-nitrogen stress in Saccharum. BMC Genomics **24**, 1-18.

Xiong C, Luo D, Lin A, Zhang C, Shan L, He P, Li B, Zhang Q, Hua B, Yuan Z, Li H, Zhang J, Yang C, Lu Y, Ye Z, Wang T. 2019. A tomato B-box protein SlBBX20 modulates carotenoid biosynthesis by directly activating *PHYTOENE SYNTHASE 1*, and is targeted for 26S proteasome-mediated degradation. New Phytologist **221**, 279-294.

Xu D, Jiang Y, Li J, Lin F, Holm M, Deng XW. 2016. BBX21, an *Arabidopsis* B-box protein, directly activates *HY5* and is targeted by COP1 for 26S proteasome-mediated degradation. Proceedings of the National Academy of Sciences **113**, 7655-7660.

Xu D, Liu X, Guo C, Lin L, Yin R. 2023b. The B-box transcription factor 4 regulates seedling photomorphogenesis and flowering in tomato. Scientia Horticulturae **309**, 111692.

Xu D, Wang H, Feng X, Ma Y, Huang Y, Wang Y, Ding J, Chen H, Wu H. 2023a. Genome-Wide Identification, Phylogenetic and Expression Analysis of the B-Box Gene Family in the Woodland Strawberry (*Fragaria vesca*). Horticulturae **9**, 842.

Xu X, Wang Q, Li W, Hu T, Wang Q, Yin Y, Liu X, He S, Zhang M, Liang Y, Zhu J, Zhan X. 2022. Overexpression of SlBBX17 affects plant growth and enhances heat tolerance in tomato. International Journal of Biological Macromolecules **206**, 799-811.

Xuefen D, Wei X, Wang B, Xiaolin Z, Xian W, Jincheng L. 2022. Genome-wide identification and expression pattern analysis of quinoa BBX family. PeerJ **10**, e4463.

Yang G, Zhang C, Dong H, Liu X, Guo H, Tong B, Fang F, Zhao Y, Yu Y, Liu Y, Lin L, Yin R. 2022. Activation and negative feedback regulation of SlHY5 transcription by the SlBBX20/21-SlHY5 transcription factor module in UV-B signaling. Plant Cell **34**, 2038-2055.

Zhang C, Wu Y, Liu X, Zhang J, Li X, Lin L, Yin R. 2022. Pivotal roles of ELONGATED HYPOCOTYL 5 in regulation of plant development and fruit metabolism in tomato. Plant Physiology **189**, 527–540.

Zhang Y, Mayba O, Pfeiffer A, Shi H, Tepperman JM, Speed TP, Quail PH. 2013. A quartet of PIF bHLH factors provides a transcriptionally centered signaling hub that regulates seedling morphogenesis through differential expression-patterning of shared target genes in *Arabidopsis*. PLoS Genetics **9**, e1003244.

Zhu Y, Zhu G, Xu R, Jiao Z, Yang J, Lin T, Wang Z, Huang S, Chong L, Zhu JK. 2023. A natural promoter variation of *SlBBX31* confers enhanced cold tolerance during tomato domestication. Plant Biotechnology Journal **21**, 1033-1043.

Zouine M, Maza E, Djari A, Lauvernier M, Frasse P, Smouni A, Pirrello J, Bouzayen M. 2017. TomExpress, a unified tomato RNA-Seq platform for visualization of expression data, clustering and correlation networks. The Plant Journal **92**, 727-735.

FIGURES

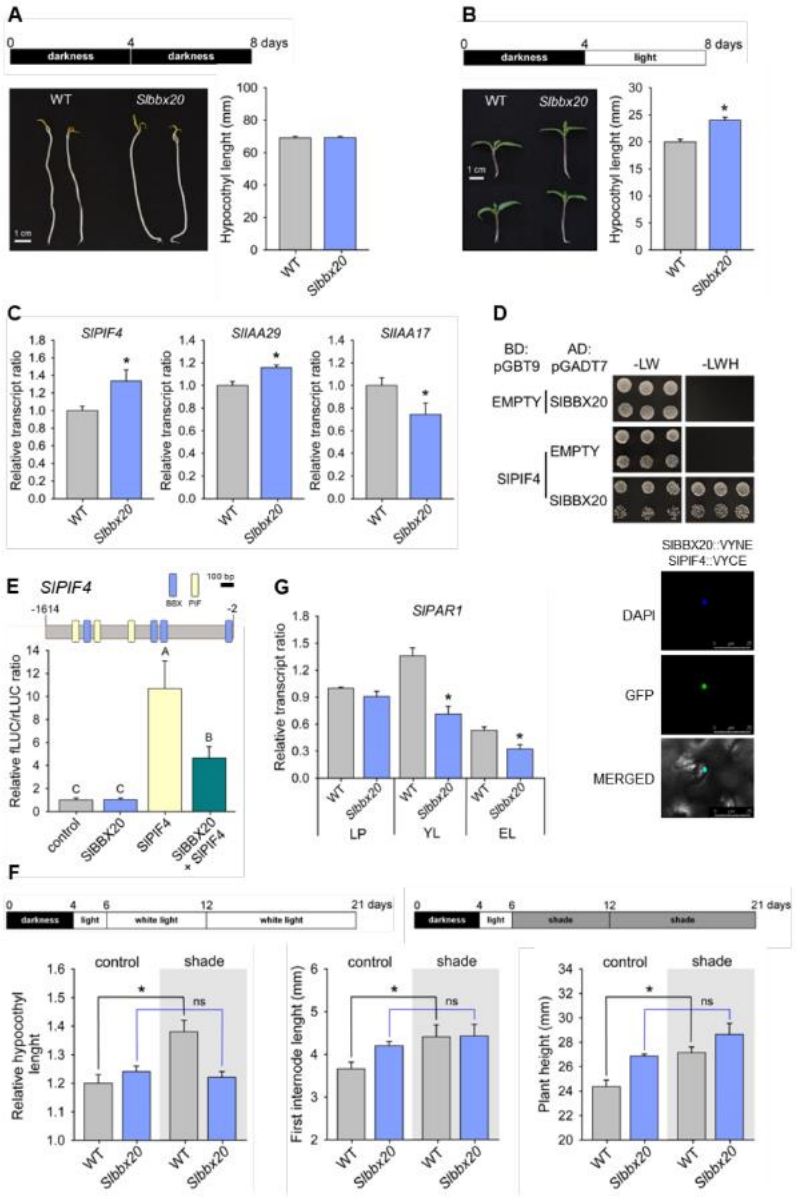

Fig. 1. *Slbbx20* seedlings are hyposensitive to light. (A) and (B) WT and *Slbbx20* seeds were sown *in vitro*, maintained for four days in darkness for germination and then, kept for additional four days in constant white light or darkness. (A) Phenotype of seedlings after dark treatment. Values are means ± SE (n=120). (B) Phenotype of seedlings after light treatment. Values are means ± SE (n=120). Asterisks indicate statistically significant difference to the corresponding WT control ($P \leq 0.05$). (C) Histograms show the relative expression of *PHYTOCHROME INTERACTING FACTOR 4* (*SlPIF4*) and *AUXIN/INDOLE-3-ACETIC ACID29* (*SlIAA29*) and *SlIAA17* signaling genes in seedling hypocotyls after light treatment. Values are means ± SE of, at least, three biological replicates relative to the respective WT control. Asterisks indicate statistically significant difference to the corresponding WT control ($P \leq 0.05$). (D) Yeast two-hybrid interactions between SlBBX20 and SlPIF4. SlBBX20 was fused to the activation domain

and SlPIF4 to the binding domain. EMPTY: autoactivation control. -LW: positive control in non-selective media without leucine and tryptophan. -LWH: selective media without leucine, tryptophan and histidine. Black boxes show three individual colonies at 10- and 100-fold dilutions. Panel below shows heterodimerization of SlBBX20 and SlPIF4 proteins by BiFC. SlBBX20::VYNE/SlPIF4::VYCE fusion proteins were transiently expressed in *Nicotiana benthamiana* leaves by infiltration with *Agrobacterium tumefaciens*. DAPI nuclear marker, GFP, bright-field merged signals are indicated above the panels. (E) BBX and PIF transcription factor motifs identified in *SlPIF4* gene promoter. BBX: CCAAT (Ben-Naim *et al*., 2006), CCACA (Gnesutta *et al*., 2017) and PIF: E-box (CANNTG, Zhang et al., 2013). Numbers indicate nucleotide positions upstream the ATG. Transactivation assay in *Nicotiana tabacum* BY-2 protoplast cells of *SlPIF4* promoter by SlBBX20 and SlPIF4. Luciferase activity is expressed as LUCIFERASE/RENILLA activity ratio relative to the negative control. Values are means ± SE (n=8). Different letters indicate significant differences ($P \leq 0.05$). (F) Shade avoidance response of *Slbbx20* seedlings. The relative hypocotyl length is expressed as the ratio between the maximum value obtained after 6 days of white light/shade treatment and the respective value at the beginning of the treatment. Internode length and plant height were measured after 15 days of shade treatment. Values are means ± SE (n=12). Asterisks indicate statistically significant difference to the corresponding WT control ($P \leq 0.05$). ns: nonsignificant (G) Relative expression of *PHYTOCHROME RAPIDLY REGULATED1* (*SlPAR1*) along leaf development stages: leaf primordia (LP), young (YL) and expanding leaves (EL) of WT and *Slbbx20*. Values are means ± SE of, at least, three biological replicates relative to the respective WT control. Asterisks indicate statistically significant difference to the corresponding WT control ($P \leq 0.05$).

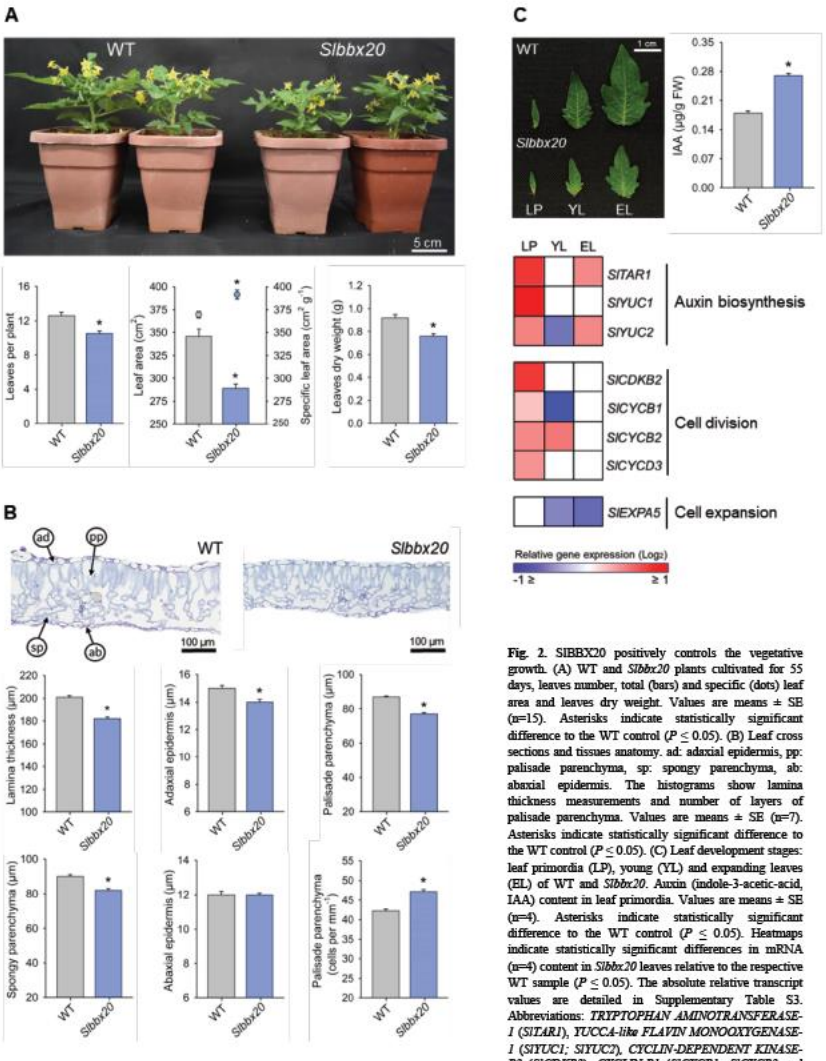

Fig. 2. SlBBX20 positively controls the vegetative growth. (A) WT and *Slbbx20* plants cultivated for 55 days, leaves number, total (bars) and specific (dots) leaf area and leaves dry weight. Values are means ± SE (n=15). Asterisks indicate statistically significant difference to the WT control ($P \leq 0.05$). (B) Leaf cross sections and tissues anatomy. ad: adaxial epidermis, pp: palisade parenchyma, sp: spongy parenchyma, ab: abaxial epidermis. The histograms show lamina thickness measurements and number of layers of palisade parenchyma. Values are means ± SE (n=7). Asterisks indicate statistically significant difference to the WT control ($P \leq 0.05$). (C) Leaf development stages: leaf primordia (LP), young (YL) and expanding leaves (EL) of WT and *Slbbx20*. Auxin (indole-3-acetic-acid, IAA) content in leaf primordia. Values are means ± SE (n=4). Asterisks indicate statistically significant difference to the WT control ($P \leq 0.05$). Heatmaps indicate statistically significant differences in mRNA (n=4) content in *Slbbx20* leaves relative to the respective WT sample ($P \leq 0.05$). The absolute relative transcript values are detailed in Supplementary Table S3. Abbreviations: *TRYPTOPHAN AMINOTRANSFERASE-1* (*SlTAR1*), *YUCCA-like FLAVIN MONOOXYGENASE-1* (*SlYUC1; SlYUC2*), *CYCLIN-DEPENDENT KINASE-B2* (*SlCDKB2*), *CYCLIN-B1* (*SlCYCB1; SlCYCB2* and *SlCYCD3*), *EXPANSIN-A5* (*SlEXPA5*) along leaf development.

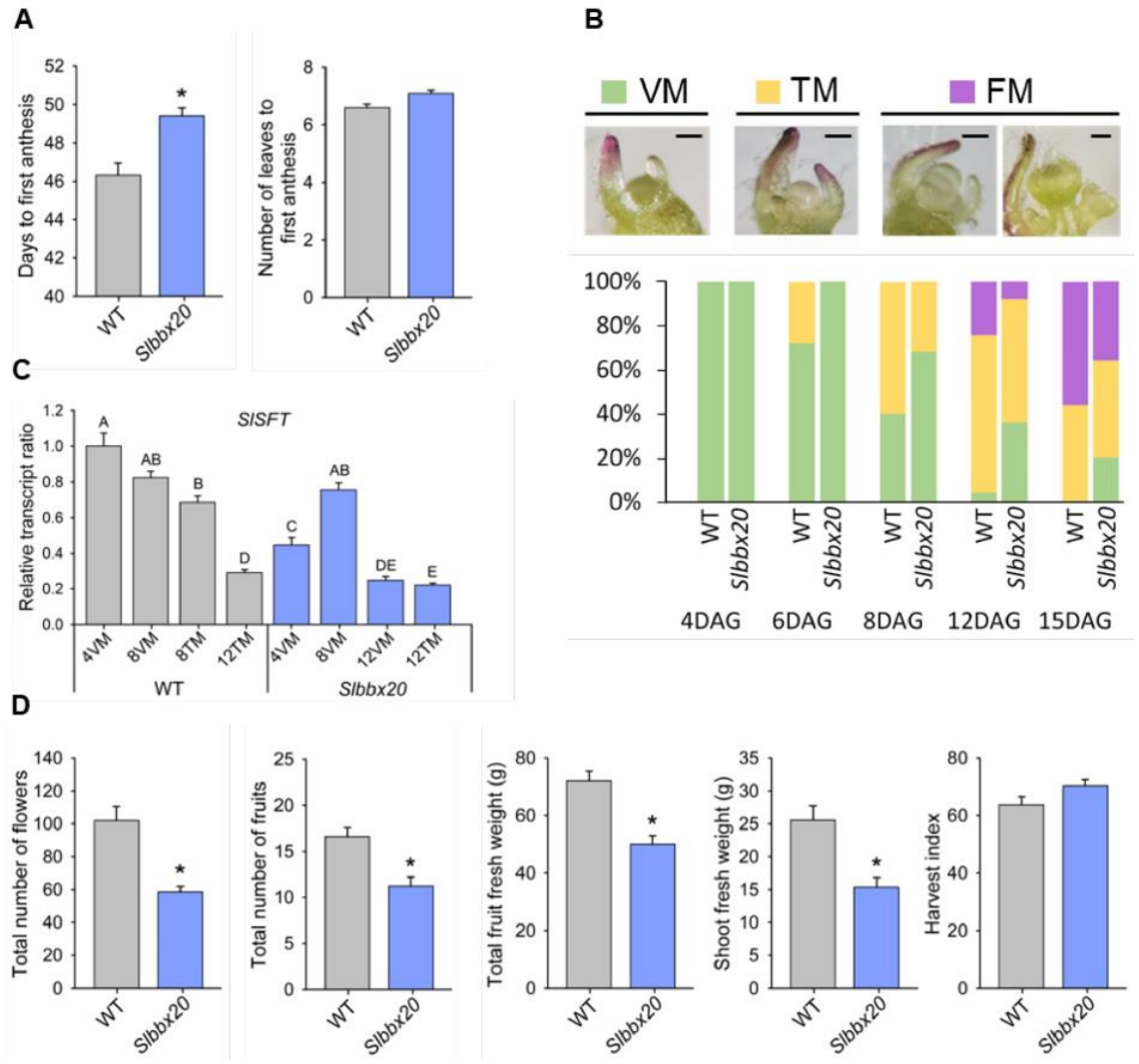

Fig. 3. SlBBX20 regulates flowering and yield. (A) Days and number of leaves until the first anthesis. Values are means ± SE (n=15). Asterisks indicate statistically significant difference to the WT control ($P \leq 0.05$). (B) The meristem from four, six, eight, twelve and fifteen days after germination (DAG), seedlings were classified as vegetative (VM), transition (TM) and floral (FM). Scale bar=100 µm. n=25. (C) Relative expression of the florigen *SINGLE FLOWER TRUSS* (*SlSFT*) in cotyledons of four, eight or twelve DAG seedlings with vegetative (VM) or transition (TM) meristems. Values are means ± SE of, at least, three biological replicates relative to the WT 4VM sample. Different letters indicate statistically significant differences ($P \leq 0.05$). (D) Yield parameters in 120-days-old plants. Values are means ± SE (n=15). Asterisks indicate statistically significant difference to the WT control ($P \leq 0.05$).

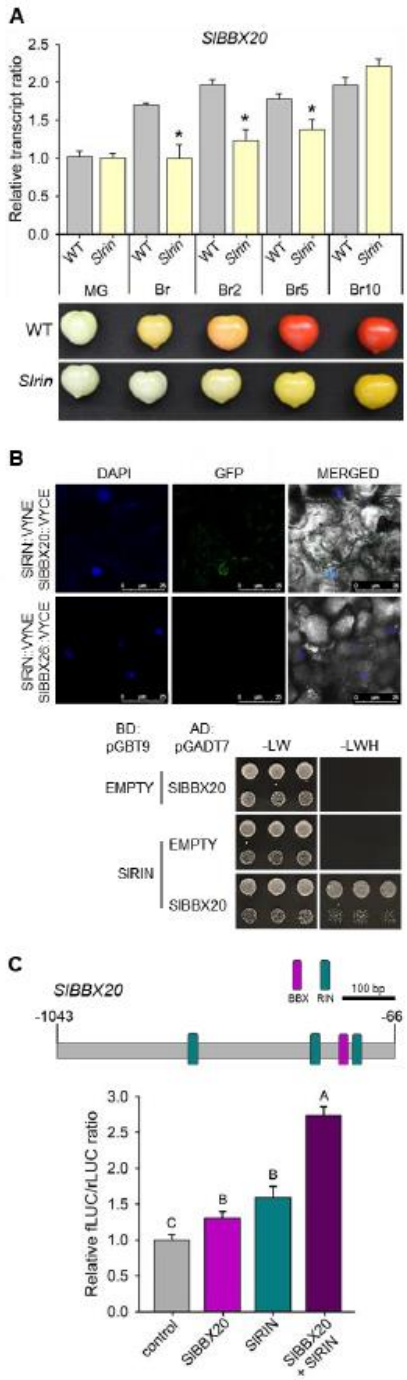

Fig. 4. SlRIN induces *SlBBX20* expression along ripening. (A) Relative expression of *SlBBX20* in fruits from the *Slrin* mutant. The bottom panel shows the corresponding phenotype of WT and *Slrin* fruits. Values are means ± SE of, at least, three biological replicates relative to the WT MG sample. Asterisks indicate statistically significant difference to the corresponding WT control ($P \leq 0.05$). (B) Heterodimerization of SlBBX20 and SlRIN proteins. SlRIN::VYNE/SlBBX20::VYCE and SlRIN::VYNE/SlBBX26::VYCE fusion proteins were transiently expressed in *Nicotiana benthamiana* leaves by infiltration with *Agrobacterium tumefaciens*. SlBBX26 was used as interaction negative control. DAPI nuclear marker, GFP, bright-field merged signals are indicated above the panels. The panel below shows yeast two-hybrid interactions between SlBBX20 and SlRIN. SlBBX20 was fused to the activation domain and SlRIN to the binding domain. EMPTY: autoactivation control. -LW: positive control in non-selective media without leucine and tryptophan. -LWH: selective media without leucine, tryptophan and histidine. Black boxes show three individual colonies at 10- and 100-fold dilutions. (C) RIN and BBX transcription factor motifs identified in *SlBBX20* gene promoter. RIN: C[CT][AT][AT][AT][AT][AT][AT][AG]G (Bianchetti *et al*., 2022), modified CArG (C[ACT][AT][AT][AT][AT][AT][AT][ATG]G, Fujisawa *et al*., 2013) and; BBX: CCAAT (Ben-Naim *et al*., 2006), CORE2 (TGTGN2-3ATG, Tiwari *et al*., 2010), CCACA (Gnesutta *et al*., 2017), G-box (CACGTG, Song *et al*., 2020), modified G-box (TACGTG, Xiong *et al*., 2019). Numbers indicate nucleotide positions upstream the ATG. Histogram shows transactivation assay in *Nicotiana tabacum* BY-2 protoplast cells of *SlBBX20* promoter by SlBBX20 and SlRIN. Luciferase activity is expressed as LUCIFERASE/RENILLA activity ratio relative to the negative control. Values are means ± SE (n=8). Different letters indicate significant differences ($P \leq 0.05$).

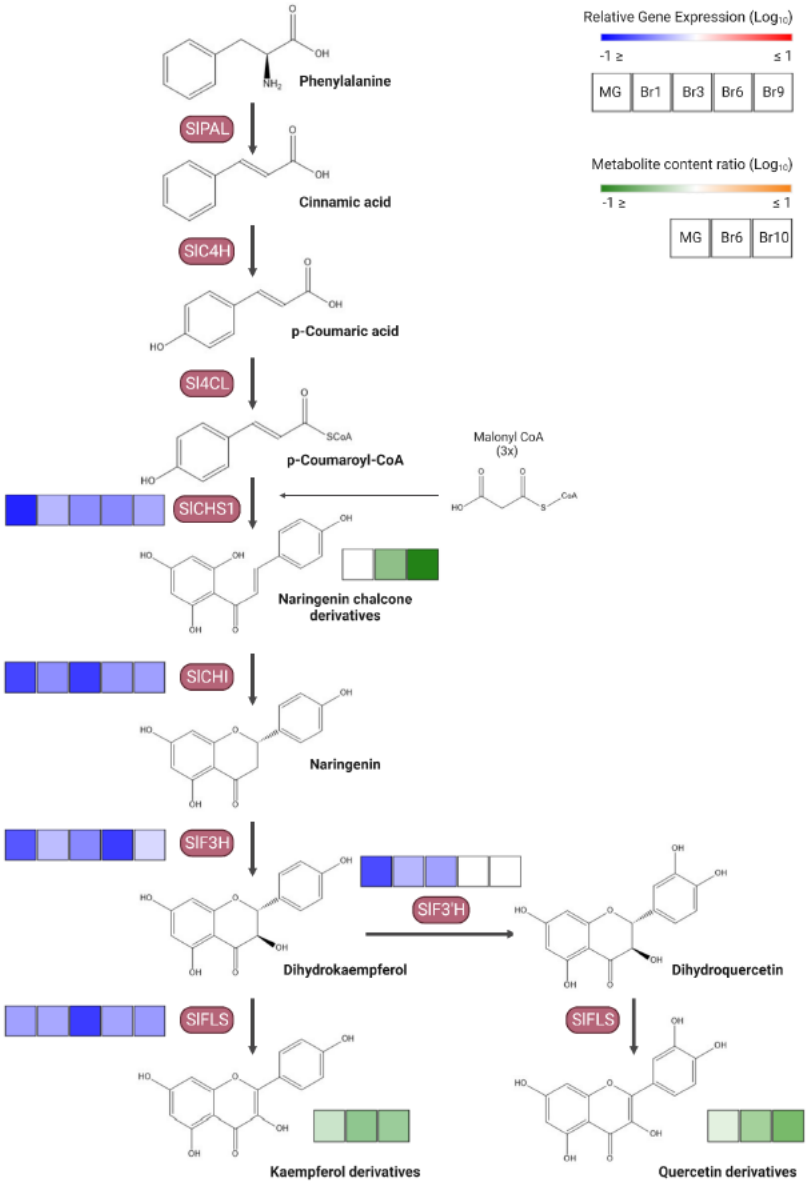

Fig. 5. SlBBX20 promotes fruit flavonoid biosynthesis. Flavonoid biosynthetic pathway. Heatmaps indicate statistically significant differences in metabolites (n=4) and mRNA (n=3) content in *Slbbx20* fruits relative to the respective WT sample ($P \leq 0.05$). The absolute metabolite and relative transcript values are detailed in Supplementary Table S5 and S6. Abbreviations: PHENYLALANINE AMMONIA-LYASE (SlPAL), CINNAMATE 4 HYDROXYLASE (SlC4H), 4-COUMARATE-CoA LIGASE (SlC4L), CHALCONE SYNTHASE 1 (SlCHS1), CHALCONE ISOMERASE (SlCHI), FLAVANONE 3-HYDROXYLASE (SlF3H), FLAVANONE 3'-HYDROXYLASE (SlF3'H), and FLAVONOL SYNTHASE (SlFLS). Created with BioRender.com.

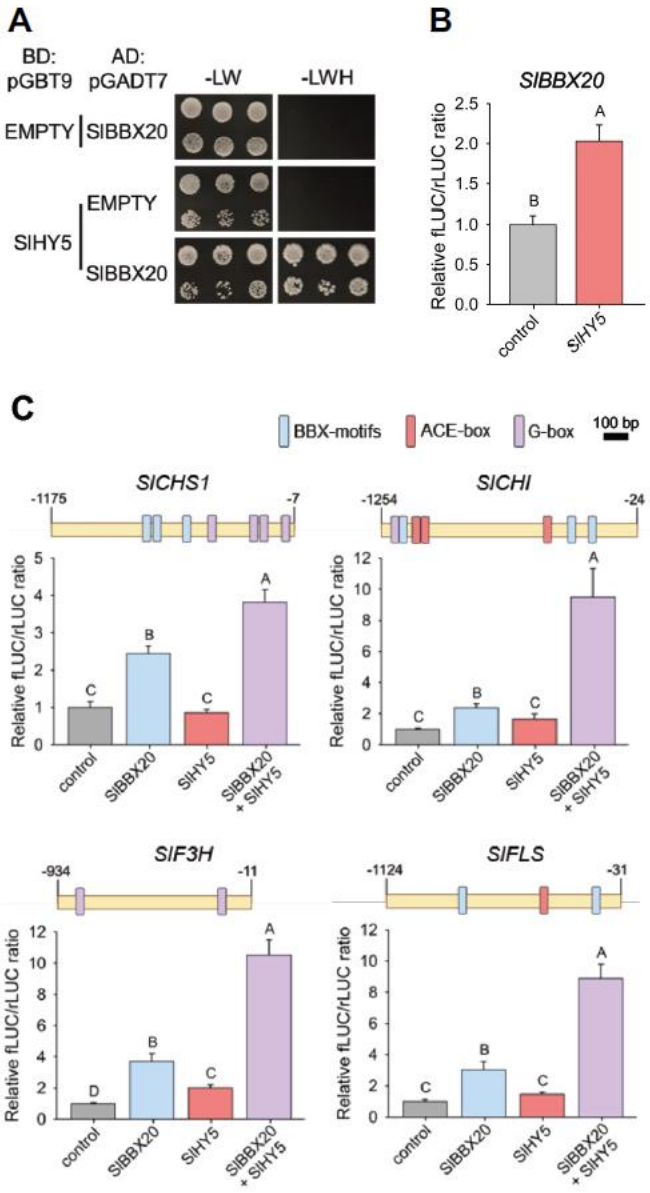

Fig. 6. SlBBX20 induces the transcriptional activity of flavonoid biosynthetic genes. (A) Yeast two-hybrid interactions between SlBBX20 and SlHY5. SlBBX20 was fused to the activation domain and SlHY5 to the binding domain. EMPTY: same autoactivation control as in Fig.1D. -LW: positive control in non-selective media without leucine and tryptophan. -LWH: selective media without leucine, tryptophan and histidine. Black boxes show three individual colony cultures at 10- and 100-fold dilutions. (B) Transactivation assay in *Nicotiana tabacum* BY-2 protoplast cells of *SlBBX20* promoter by SlHY5. Luciferase activity is expressed as LUCIFERASE/RENILLA activity ratio relative to the negative control. Values are means ± SE (n=8). Different letters indicate significant differences ($P \leq 0.05$). (C) BBX and HY5 binding motifs in flavonoids biosynthetic gene promoters (yellow lines) are shown. BBX motifs: CCAAT (Ben-Naim *et al*., 2006), CORE2 (TGTGN$_{2\text{-}3}$ATG, Tiwari *et al*., 2010), CCACA (Gnesutta *et al*., 2017). HY5 motif: ACE-box (ACGT, Wang *et al*., 2021). Common motifs: G-box (CACGTG,

Song *et al*., 2020) and modified G-box (TACGTG, Xiong *et al*., 2019). Numbers indicate nucleotide positions upstream the ATG. Histograms show the transactivation assay in *Nicotiana tabacum* BY-2 protoplast cells of flavonoids biosynthetic gene promoters by SlBBX20 and/or SlHY5 as effectors. Luciferase activity is expressed as LUCIFERASE/RENILLA activity ratio relative to the negative control. Values are means ± SE (n=8). Different letters indicate significant differences ($P \leq 0.05$).

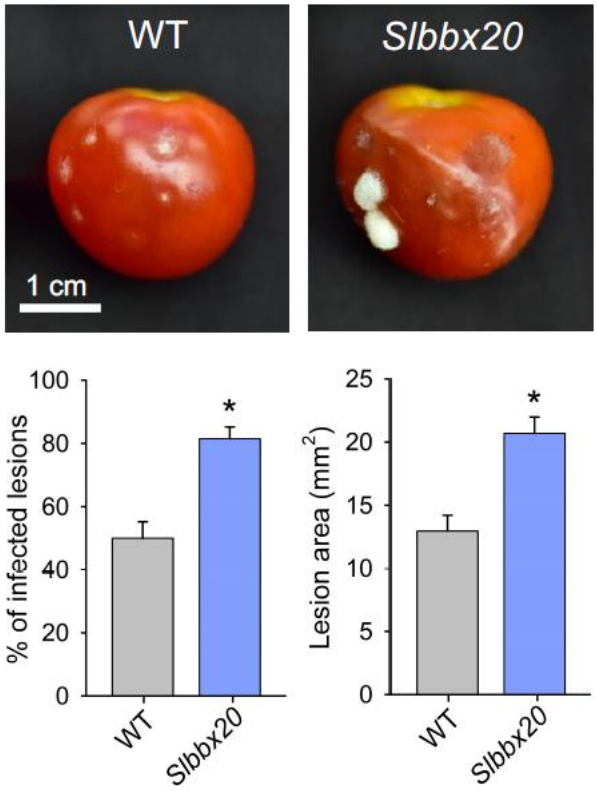

Fig. 7. SlBBX20 participates in defense response. Representative WT and *Slbbx20* fruits at Br10 stage 48 hours after infection with *Botrytis cinerea.* The fruits were punctured and inoculated with fungus conidia. Histograms show disease incidence and severity. Values are means ± SE (n=15). Asterisks indicate statistically significant difference to the WT control ($P \leq 0.05$).

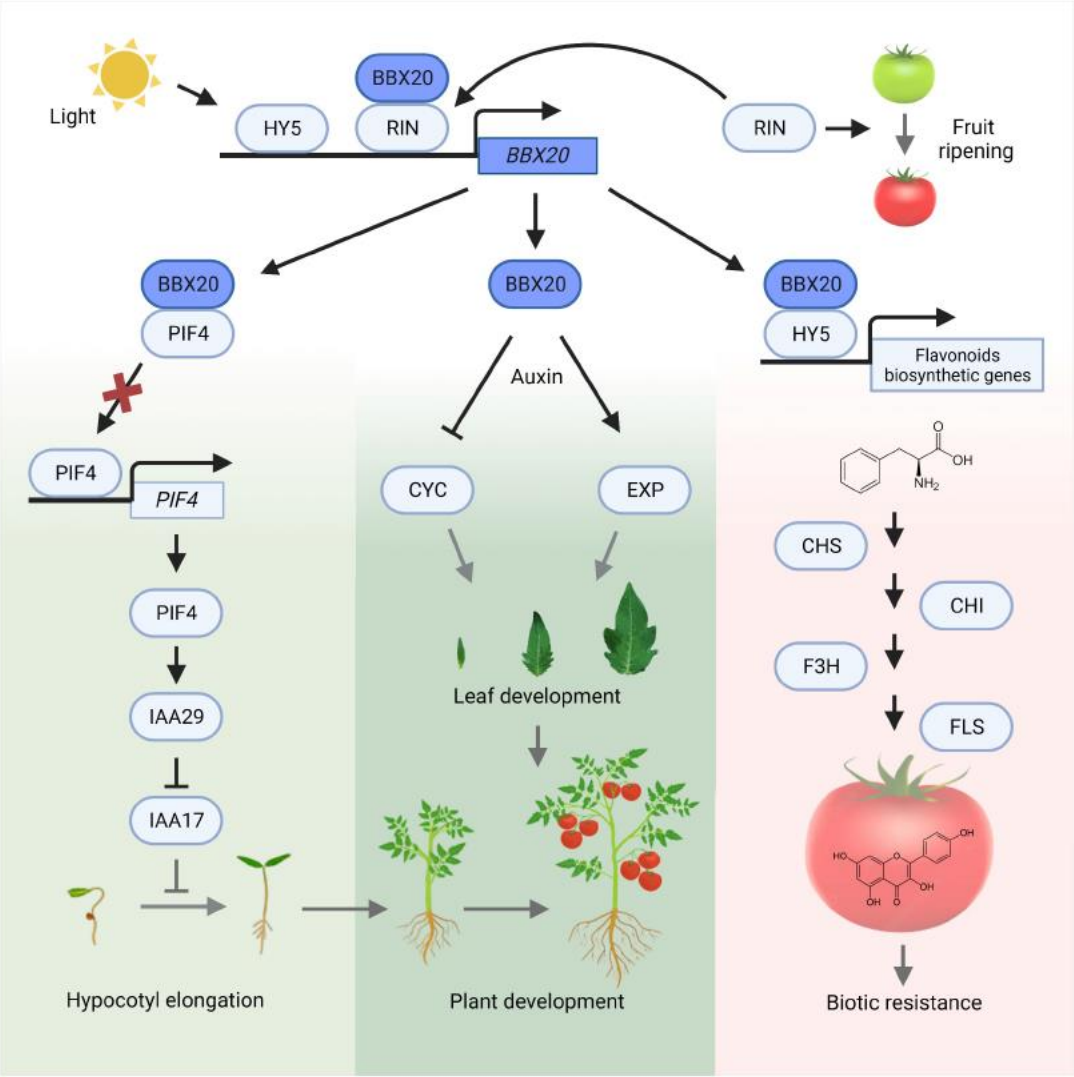

Fig. 8. SlBBX20 regulates several processes along plant development. SlBBX20 molecular mechanisms controlling tomato plant development and fruit quality. The binding of SlRIN to *SlBBX20* promoter and SlHY5 to the promoters of flavonoids biosynthetic genes were demonstrated through chromatin immunoprecipitation follow by qPCR (Lira *et al*., 2020; Wang *et al*., 2021), respectively. Abbreviations: ELONGATED HYPOCOTYL 5 (HY5), PHYTOCHROME INTERACTING FACTOR 4 (PIF4), AUXIN/INDOLE-3-ACETIC ACID (IAA29, IAA17), CYCLIN (CYC), EXPANSIN (EXP), RIPENING INHIBITOR (RIN), CHALCONE SYNTHASE 1 (CHS), CHALCONE ISOMERASE (CHI), FLAVANONE 3-HYDROXYLASE (F3H) and FLAVONOL SYNTHASE (FLS). Grey and black arrows indicate physiological processes and regulatory links, respectively. Bar/arrow line end represents negative/positive interactions. Created with BioRender.com.